Modelling wind farm effects in HARMONIE-AROME (cycle 43.2.2) – part 1: Implementation and evaluation

Jana Fischereit[1], Henrik Vedel[2], Xiaoli Guo Larsén[1], Natalie E. Theeuwes[3], Gregor Giebel[1], and Eigil Kaas[2]

[1]DTU Wind and Energy Systems, Frederiksborgvej 399, 4000 Roskilde, Denmark
[2]Danish Meteorological Institute, Lyngbyvej 100, 2100 Copenhagen, Denmark
[3]Royal Netherlands Meteorological Institute (KNMI), Utrechtseweg 297, 3731 GA De Bilt, The Netherlands

Correspondence: Jana Fischereit (janf@dtu.dk)

Abstract. With increasing number and proximity of wind farms, it becomes crucial to consider wind farm effects (WFE) in the numerical weather prediction (NWP) models used to forecast power production. Furthermore, these WFE are also expected to affect other weather-related parameters at least locally. Thus, we implement the explicit wake parameterization (EWP) in the NWP model HARMONIE-AROME (hereafter HARMONIE) along-side the existing wind farm parameterization (WFP) by Fitch et al. (2012) (FITCH). We evaluate and compare the two WFPs against research flight measurements as well as against similar simulations performed with the Weather Research and Forecasting model (WRF) using case studies. The case studies include a case for WFE above a wind farm as well as two cases for WFE at hub height in the wake of farms. The results show that EWP and FITCH have been correctly implemented in HARMONIE. For the simulated cases, EWP underestimates the WFE on wind speed and strongly underestimates the effect on turbulent kinetic energy (TKE). FITCH agrees better with the observations and WFE on TKE are particularly well captured by HARMONIE-FITCH. After this successful evaluation, simulations with all wind turbines in Europe will be performed with HARMONIE and presented in the second part of this paper series.

1 Introduction

Wind turbines extract kinetic energy from the atmospheric flow to produce electricity. Thereby, they reduce the wind speed upstream, referred to as blockage effect, and downstream, referred to as wake effect, and sometimes increase the wind speed on the sides, referred to as speed-up effect (e.g. Fischereit et al., 2022a). In addition, they increase turbulence both directly through tip vortices, as well as indirectly through shear production. Hence, wind and turbulence profiles are modified around wind farms and consequently also local temperature and humidity profiles (e.g. Siedersleben et al., 2018; Baidya Roy and Traiteur, 2010).

Since wind turbines increase in number and size both on- and offshore (IRENA, 2019), their impact on numerical weather prediction (NWP) can no longer be generally ignored. According to a recent review by Fischereit et al. (2022a), the Weather Research and Forecasting (WRF) model is the most wide-spread applied model equipped with a wind farm parameterization (WFP). Extensive validation of WRF with the built-in WFP by Fitch et al. (2012), hereafter 'FITCH', has been performed as summarized in Fischereit et al. (2022a). Besides WRF + FITCH, the Explicit Wake Parameterisation (Volker et al., 2015), hereafter EWP, is the second most frequently applied WFP in WRF according to the review in Fischereit et al. (2022a). In addition, FITCH has been implemented in other NWP models, among others in HARMONIE-AROME (Bengtsson et al., 2017, https://hirlam.github.io/HarmonieSystemDocumentation), hereafter HARMONIE, by van Stratum et al. (2022).

While WRF+WFP has been extensively applied and verified as summarized in Fischereit et al. (2022a), WFPs in HARMONIE are still relatively unexplored. Since HARMONIE is used by at least 11 national weather services in Europe, it is relevant to also integrate WFE in HARMONIE. van Stratum et al. (2022) started this process with the implementation of FITCH. They evaluated a one-year long simulation against measurements of power production, from lidar and mast, as well as in a case study against aircraft measurements. They showed that using FITCH provided a more realistic representation of the atmosphere near wind farms than a simulation without WFP. In this study, we extend the work by van Stratum et al. (2022) by implementing the EWP into HARMONIE. Having two WFPs available is advantageous, because it allows one to create an ensemble of possible wind farm effects (WFE), highlighting the uncertainty of the forecast.

Previous studies have explored the differences between wind farm effects predicted by FITCH and EWP in WRF. Pryor et al. (2020) noted in their nine month long study of the U.S. Midwest that capacity factors were lower for simulations with FITCH than with EWP. They also found that wind speed deficits and TKE enhancements extended over a larger area for FITCH than for EWP. Similar conclusions were drawn by Shepherd et al. (2020), who performed a yearlong simulation for Iowa. They also noted that the differences lead to differences in impacts on near-surface climate variables. Fischereit et al. (2022b) compared high-resolution RANS simulations with WRF+WFP simulations and noted that EWP underestimated the wake wind speed deficits between farms, while FITCH performed reasonably well. Larsén and Fischereit (2021) found that above a wind farm both EWP and FITCH can capture the wind speed deficit fairly well compared to measurements. However, EWP significantly underestimated TKE above the farm. This study builds upon and extends the previous studies on comparing EWP and FITCH by comparing with actual measurements within the wake.

The work is divided into two parts. Part 1 is presented in this manuscript and describes the implementation of EWP in HARMONIE, as well as the comparison with the WRF results and flight measurements for three case studies. The specific objectives of part 1 are given below. Part 2, presented in Fischereit et al. (2023a), deals with the setup of a wind turbine database for Europe, the long-term evaluation of the HARMONIE simulations as well as the sensitivity of the forecast to the applied WFP.

Part 1 in the present manuscript has three objectives: (1) Ensuring that EWP and FITCH are correctly implemented in HARMONIE, (2) evaluate how wind farm effects are manifested and transported in HARMONIE and verify that by comparing to WRF and (3) check how well the wind farm effects in both HARMONIE and WRF agree with flight measurements in the wake and above wind farms. To archive those objectives the manuscript is structured as follows: key features of EWP and

the implementation of EWP into HARMONIE are described in Sect. 2.1. The model setups for HARMONIE and WRF for the simulations are described in Sect. 2 and the results and comparisons are shown in Sect. 3, and discussed in Sect. 4 and concluded in Sect. 5.

2 Modelling frameworks and case studies

In the following the applied WFPs, models and model setups are described. Sect. 2.1 describes the characteristics of the EWP and highlights the differences to the more widely used FITCH (Fitch et al., 2012). In Sect. 2.2 and Sect. 2.3 introduces the two applied NWP models, HARMONIE and WRF, respectively. The investigated case studies are described in Sect. 2.4 and Sect. 2.5.

2.1 Implementation of EWP in HARMONIE

The theory and derivation of EWP are described in detail in Volker et al. (2015). For convenience we repeat the main concepts here.

To parameterize the effect of wind farms on the atmosphere, EWP imposes an elevated momentum sink or drag force on a control volume $\Delta\forall$ of the flow U, which acts on the rotor area A_r and is proportional to the thrust coefficient C_T:

$$\overline{f}_t = \frac{1}{2} C_T U^2 A_r / \Delta\forall. \tag{1}$$

This is similar to the FITCH parameterization. However, in contrast to FITCH, EWP accounts for a subgrid scale vertical wake expansion. The idea behind this is that due to the size of the mesoscale grid cell of typically 1–5 km^2, the wind turbine wake has expanded vertically when reaching the grid cell boundary. To account for this effect, EWP builds upon classical wind turbine wake theory, by assuming an exponential expansion based on an effective length scale σ_e to define the drag force at grid cell x, y, z:

$$f_{xyz} = N_t \sqrt{\frac{\pi}{8}} \frac{C_T r_h^2 |\overline{u}_{rh_{xy}}|^2}{\Delta x \Delta y \sigma_e} \exp\left[\frac{1}{2}\left(\frac{z_z - h}{\sigma_e}\right)^2\right] \tag{2}$$

Here, N_t is the number of turbines per grid cell, r_h is the rotor radius $= 0.5d$ with d being the rotor diameter, $\overline{u}_{rh_{xy}}$ denotes the horizontal wind speed $\overline{u}_r = \left(\overline{u}_1^2 + \overline{u}_2^2\right)^{0.5}$ with 1 and 2 denoting the wind components in the two horizontal directions at hub height h averaged over one grid cell and a finite time increment, as indicated by the overbar, z_z is the height of the model level z and the thrust coefficient is used as a function of the wind speed at hub height $C_T = C_T(\overline{u}_{rh})$. The effective length scale, σ_e, is related to the model grid size ($L = 0.5\Delta x$), the turbulent diffusion coefficient from mesoscale turbulence scheme (K) and an initial length scale that represents the unresolved wake expansion in the near wake $\sigma_h = f_r r_h$ with f_r being a tuneable wake expansion scaling factor:

$$\sigma_e = \frac{\overline{u}_{rh}}{3KL}\left[\left(\frac{2K}{\overline{u}_{rh}}L + \sigma_h^2\right)^{3/2} - \sigma_h^3\right] \tag{3}$$

Using the wind direction, WD, the drag force f_{xyz} is split into the two wind components:

$$\overline{f}_{1,xyz} = f_{xyz}\cos(WD_{xyz}) \quad \text{and} \quad \overline{f}_{2,xyz} = f_{xyz}\sin(WD_{xyz}) \tag{4}$$

Another difference between FITCH and EWP is the treatment of turbulent kinetic energy (TKE) within these schemes. For EWP Volker et al. (2015) assumes that the heterogeneous part of the mean flow (e.g. organized motions) is part of the mean flow kinetic energy and not part of random TKE. Based on that, the remaining addition of TKE due to the rotation of wind turbines is negligible in a mesoscale model. In FITCH such a distinction is not made and thus an explicit TKE source term is added to the mesoscale model equations (Fitch et al., 2012). In both the EWP and the FITCH scheme, wind turbines are an implicit source of TKE through shear generated turbulence arising from the turbine wake. More details on the derivation for EWP are given in Volker et al. (2015) and more discussions on the difference between FITCH and EWP can be found in e.g. Fischereit et al. (2022a).

The implementation of EWP in HARMONIE follows the implementation of FITCH as described in van Stratum et al. (2022). The only difference is that for EWP the TKE tendencies are not modified, and a different drag force is used. The turbulent diffusion coefficient, K, is used to calculate the wake expansion. K is derived from the stability corrected turbulence length scale ℓ (Lenderink and Holtslag, 2004) and TKE from the planetary boundary layer (PBL) scheme in HARMONIE:

$$K = \ell \cdot \sqrt{\mathrm{TKE}} \tag{5}$$

For the implementation of Eq. 4, WD is not the true wind direction, since u and v are grid-following in HARMONIE, and are thus not necessarily aligned with the cardinal directions north-south and east-west.

This implementation is similar to the implementation of EWP in WRF except that turbulent diffusion coefficient, K, is different, since it is provided by a different PBL scheme. Having EWP implemented in HARMONIE allows for comparisons of different WFPs in HARMONIE as well as comparisons of WFE in HARMONIE and WRF.

2.2 HARMONIE

We implement EWP in HARMONIE-AROME cycle 43.2.2. HARMONIE is a nonhydrostatic, convection permitting limited-area NWP model that is developed within the HIRLAM-C consortium (Bengtsson et al., 2017, https://hirlam.github.io/HarmonieSystemDoc The dynamics are based on the fully compressible Euler equations (Simmons and Burridge, 1981), which are solved numerically using a semi-Lagrangian advection scheme with semi-implicit time stepping (Bénard et al., 2010). The physical parameterizations include a multiband radiation scheme, prognostic equations for liquid and solid hydrometeors, a prognostic equation for turbulent kinetic energy, and a mass-flux-based shallow convection scheme called EDMFm. Surface physics is modelled using the SURFEX scheme (Masson et al., 2013). For further details on HARMONIE see Bengtsson et al. (2017).

Here we use the model grid design of the operational NWP setup at the Danish Meteorological Institute (DMI): We simulate the Northern Europe DMI domain ~~NEA~~A (NEA), which covers all of Scandinavia, UK, Iceland and parts of Germany, and

is centered around 60°N and 7°E (Fig. 1b). It has a horizontal resolution of 2.5 km and 65 vertical layers, running from the surface up to 10 hPa. The lowest 10 full levels are most relevant for this study, located approximately at 12 m, 38 m, 63 m, 89 m, 117 m, 146 m, 177 m, 211 m, 247 m, 287 m height above the ground. These levels along with those defined in WRF and rotor areas for the different turbine types are shown in Fig. 2.

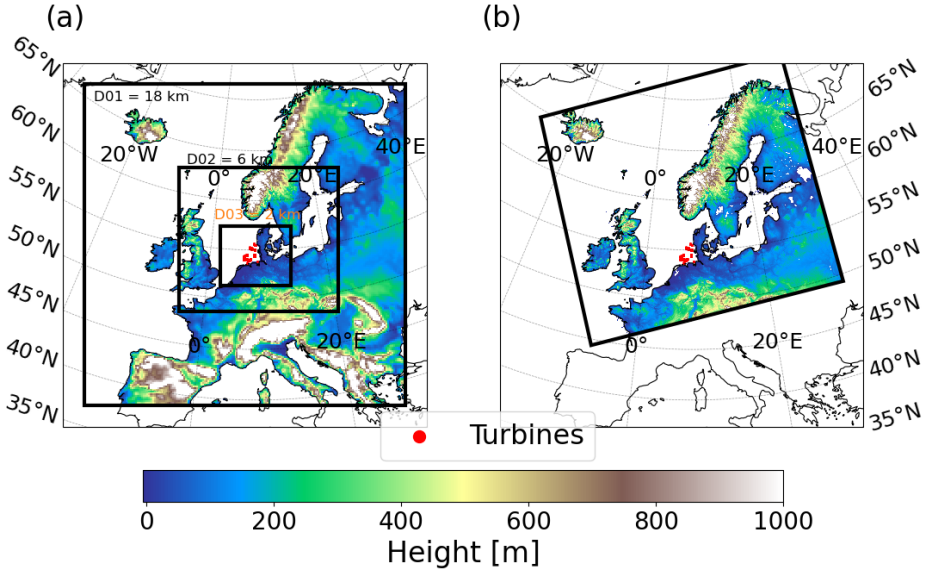

Figure 1. (a) Nested WRF domain and (b) HARMONIE domain 'NEA' and employed in this study.

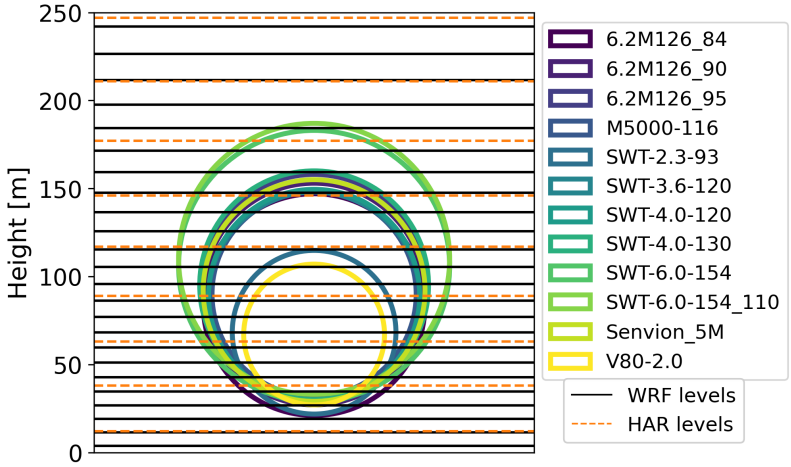

Figure 2. WRF (black solid) and HARMONIE (orange dashed) model levels and rotor areas of the different turbine types used in this study.

We run HARMONIE in forecasting mode ~~and use hourly IFS fields from ECMWFs global forecast model~~ using hourly boundary fields from the Integrated Forecasting System (IFS) global model at ECMWF as lateral boundary conditions. A warm-up period of 7 days prior to the case study days (Sect. 2.4) is used to spin-up the simulations. The long spin-up period is needed due to advanced 3D-VAR data assimilation used in HARMONIE. After the spin-up period using 3-hour cycling, 24-hour forecasts are made at 00 and 12 UTC. The data assimilation includes surface synoptic observation (SYNOP) pressures, radiosonde winds, temperatures and humidities, buoy pressures, aircraft winds and temperatures (AMDAR). In addition several types of surface and near surface data are assimilated. For sea surface temperatures OSTIA (Donlon et al., 2012) is used. The evaluated forecast was performed at the closest synoptic hour, which corresponds to 12:00 for the three test cases. We use the parameterizations and settings mostly corresponding to the operational forecasts at DMI. The only exception is the use of WFPs and the number and type of assimilated observations. A summary of all settings is given in Table 1.

2.3 WRF

We apply WRF 4.2.2 (Skamarock et al., 2019) in a nested domain setup with the corresponding spatial resolutions 18 km, 6 km and 2 km shown in Fig. 1a. We use 80 non-equidistant vertical model levels with more levels in the lowest 200 m of the atmosphere around the rotor (Fig. 2, Table 1). We run WRF in hindcast mode and use ERA5 data as the initial and boundary conditions. More details on the physical schemes are given in Table 1. The settings follow mostly those in Larsén and Fischereit (2021), since in that study good agreement was found for the mean wind structures between the simulations and three types of measurements.

All WRF simulations are initialized at midnight and run for 24 hours, except for the simulation on 15 October 2017. For the simulation on 15 October 2017, it was investigated whether initialization at 00:00 or 06:00 would show better results. The simulation initialized on 00:00 underestimated the wind speed, and therefore we used 06:00 as the initial time. Sensitivity tests show that for stable cases the later initialization helps to better capture transient meteorological conditions by properly introducing the initial conditions to the simulation. A similar behaviour was reported in Larsén and Fischereit (2021) for 14 October 2017 and could be solved by initializing the simulations at 06:00. Since the analysis presented in this study starts after 12:00 a spin-up time of 6 hours is still maintained. The other simulations use a spin-up time of around 12 hours.

2.4 Case studies

We investigate three case studies (Table 2) to evaluate the implementation of EWP in HARMONIE. One of the main reasons for choosing the three cases is that high resolution open access flight measurements conducted within the German WIPAFF project (Bärfuss et al., 2019) are available. These cases also include a variety of conditions of wind speed, wind direction, and stability, which enable us to evaluate the WFP performance in different background conditions. In addition, the cases differ in the type of WFE that was measured: within the wake at around hub height or above the wind farm. Thus, by choosing these cases, the implemented WFP can be evaluated for different effects. This also extends the evaluation performed in van Stratum et al. (2022), which only included one evaluation within the wake at hub height. In addition, we here focus also on other parameters, especially TKE, which was not included in the previous evaluation.

Table 1. Model settings for HARMONIE and WRF.

Parameter	HARMONIE	WRF
Version	43.2.2 with Fitch and EWP implemented	4.2.2 with EWP implemented
Spatial settings		
Domain (Fig. 1)	2.5 km uniformly (1200 x 1080 pts)	One-way nested: D1: 18 km (202 x 202 pts), D2: 6 km (301 x 271 pts), D3: 2 km (394 x 334 pts)
Center location	60°N and 7°E	55.5°N and 6°E
Vertical levels (Fig. 2)	65 levels, $\Delta z \approx 26$ m up to 117 m	80 levels, $\Delta z \approx$ 10–25 m up to 200 m
Temporal settings		
Simulation length	7 days (8 days for 15 October 2017)	24 hours
Spin-up	7.5 days	12 hours (6 hours for case study 15 October 2017)
Update interval	Data assimilation every 3 hours, 24 h forecasts at 00:00 and 12:00	Boundary conditions every 6 hours, spectral nudging applied above the boundary layer
Output interval	15 min	10 min
Initialization and boundary		
Forcing data	ECMWF daily forecasts (hourly, 18 km horizontal, 137 vertical levels)	Reanalysis: ERA5 (Hersbach et al., 2018) on pressure levels
Terrain data	Combination of local high resolution datasets	GMTED2010 (Danielson and Gesch, 2011)
Land use data	Combination of local high resolution datasets	ESA CCI[1]
Sea surface temperature	OSTIA (Donlon et al., 2012)	OSTIA (Donlon et al., 2012)
Physics scheme		
Microphysics	ICE-3: Pinty and Jabouille (1998), Lascaux et al. (2006), Bouteloup et al. (2011), Bengtsson et al. (2017)	Thompson et al. (2008) (option 8)
Radiation	Long-wave: 16 band RRTM. Short-wave: Bengtsson et al. (2017)	RRTMG Iacono et al. (2008) (option 4)
Cumulus	Deep convection resolved. Shallow convection: EDMFm (Neggers et al., 2007; Siebesma et al., 2007; de Rooy and Siebesma, 2008; de Rooy and Pier Siebesma, 2010)	For D1 only: Kain (2004) (option 1)
Land surface	SURFEX (Masson et al., 2013)	Noah LSM (Tewari et al., 2004) (option 2)
Planetary boundary layer	Turbulence parameterisation with HARATU (de Rooy et al., 2022)	MYNN2.5 (Nakanishi and Niino, 2009) (option 5)
Wind farm parameterization	EWP with f_r =1.7 FITCH with $f_{TKE} = 1$	EWP with f_r =1.7 FITCH with $f_{TKE} = 1$

[1] Available from https://www.esa-landcover-cci.org/

The flight tracks during the three cases in relation to the corresponding wind farms are shown in Fig. 3. The case study on 14 October 2017 (blue lines in Fig. 3) is used to evaluate the performance of the simulations above a wind farm. This case follows up on existing analysis in Larsén and Fischereit (2021) and Siedersleben et al. (2020). The other two cases evaluate the wake of the farm around hub height (purple and orange lines in Fig. 3). Background and evaluation objective are summarized in Table 2.

Table 2. Investigated case studies. Background conditions refer to the first transect upwind of the farm.

Date	Wind farms	Flight height (mean height)	Background conditions	Evaluation objective
08 August 2017	Amrumbank West, Nordsee Ost and Meerwind Süd/Ost	Wake at hub height (91 m)	80° (E); 13 ms^{-1}	wake with temperature effect
14 October 2017	Gode Wind 1+2 and Nordsee One	Above wind farm (250 m)	250° (W-SW); 15 ms^{-1}	effects above the farm
15 October 2017	Gode Wind 1+2 and Nordsee One	Wake slightly above hub height (122 m)	190° (S-SW); 11 ms^{-1}	wake without temperature effect

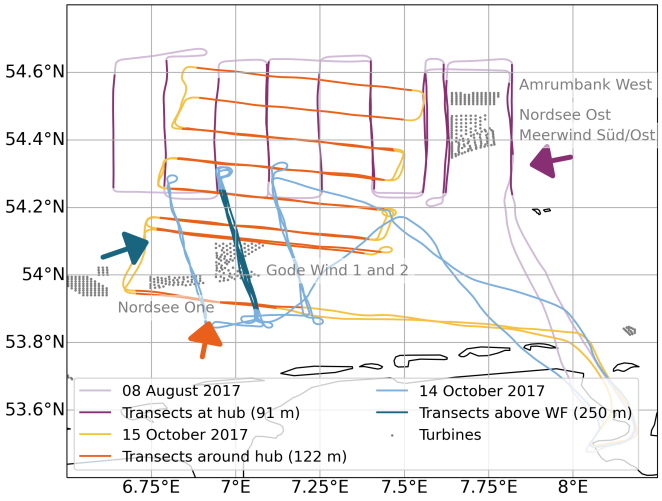

Figure 3. Flight tracks (brighter lines) and focus transects (darker lines) for the three case studies 08 August 2017 (purple), 14 October 2017 (blue), and 15 October 2017 (orange) along with the turbines of interest in that area (gray) and the mean wind speed and direction for the cases (colored arrows) derived from the first upwind transects with respect to the farm (Table 2).

The raw flight data was divided into transects, which are shown as darker stretches in Fig. 3. These transects were approximately perpendicular to the mean direction of the wind upwind. The mean flight height for the three case studies were 91 m, 122 m and 250 m. The transect flight data are sampled at a frequency of 100 Hz with the aircraft ground speed being 66 ms^{-1} (Platis et al., 2018), which corresponds to a spatial resolution of 0.66 m. The data include, among others, the three

wind components (u, v, and w), temperature, and humidity. We calculate TKE using the standard deviation, σ, of the three wind components: $TKE = 0.5 \cdot (\sigma_u^2 + \sigma_v^2 + \sigma_w^2)$. For the calculating the standard deviations, we use the same data window of 2 km, as in Larsén and Fischereit (2021) and close to that used in Platis et al. (2020).

In addition to the WIPAFF measurements, we also use synthetic aperture radar (SAR) data taken from https://science.globalwindatlas.info/#/map (Badger et al., 2022) to evaluate the general meteorological situation during the case studies. The SAR images are retrieved from ENVISAT and combined with an empirical transfer function to derive the neutral 10 m wind speed from the radar backscatter of small locally generated waves. All the SAR images shown in Sect. 3 are made up of more than one SAR scene recorded at around 17:00 UTC. The area in the SAR scene does not always cover the full flight track but serves to assess the background conditions.

2.5 Wind turbines

The position and types of wind turbines are taken from Larsén and Fischereit (2021) for both the HARMONIE and WRF simulations. The rotor areas with respect to the vertical grid for the various turbines are shown in Fig. 2 and the positions are shown in Fig. 1, respectively. Since the flight measurements (Sect. 2.4) were conducted in 2017, we only include wind turbines present in the North Sea at that time. For the case studies, we focus on four wind farms (Table 2): for the case studies on 14 October 2017 and 15 October 2017 on Gode Wind 1+2 and Nordsee One, and for the case study on 08 August 2017 on Amrumbank West, Nordsee Ost and Meerwind Süd/Ost (Fig. 3). Gode Wind 1+2 and Nordsee One are equipped respectively with 110 m tall SWT-6.0-154 wind turbines (SWT-6.0-154_110 in Fig. 2) and 90 m tall 6.2M126 wind turbines (6.2M126_90 in Fig. 2). In Amrumbank West and Meerwind Süd/Ost 88 m tall SWT-3.6-120 wind turbines are installed. Nordsee Ost is equipped with 95 m tall 6.2M126 wind turbines. The thrust and power curves of these three wind turbine models for the complete range of operating wind speeds are shown in Fig. 4. Note that C_T is always smaller or equal to 1, since below 3 ms^{-1} or 4 ms^{-1}, depending on the turbine model, the turbines are not operating and therefore C_T is not defined. The C_T curves cannot be extrapolated to lower wind speeds.

The turbines are assigned to the grid cells in WRF and HARMONIE. Figure 5 shows, how many turbines are assigned to each grid cell around the wind farms of interest.

We simulate three scenarios for each case study (Table 2) for both the HARMONIE and WRF simulations. The three scenarios are (1) a scenario without WFEs included (denoted 'NWF'), (2) a scenario with the parameterization by Fitch et al. (2012) (denoted 'FITCH') and (3) a scenario with the EWP parameterization (denoted 'EWP'). For FITCH we use a turbulent kinetic energy (TKE) factor of 1 in WRF to make it comparable to the implementation in HARMONIE, which does not include a TKE factor. The correction factor for TKE was introduced following the discovery of a bug in the implementation of turbine-generated TKE in the WRF model (Archer et al., 2020). It is an empirical factor that was derived based on the best agreement between a LES simulation and a WRF-FITCH simulation. Using this comparison Archer et al. (2020) suggested to use a factor of 0.25. However, a subsequent study by Larsén and Fischereit (2021) found inconclusive results when comparing simulations using correction factors of 0.25 and 1 with measurements. Thus, while a correction factor of 1 deviates from the default, the 'best' choice is still unclear. Hence, it is reasonable to use a correction factor of 1, i.e. no correction factor, here. For EWP

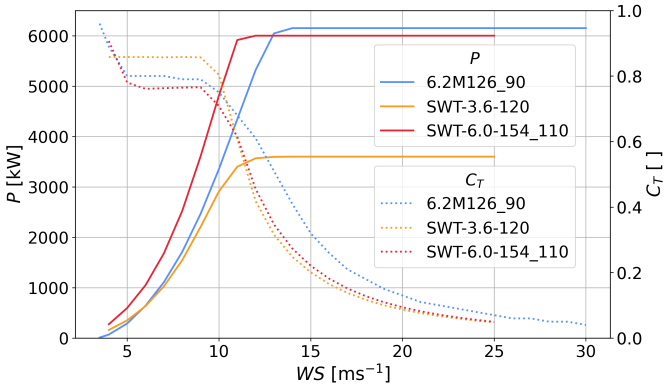

Figure 4. Thrust and power curves for the turbine types of the four wind farms of interest. Note that the power and thrust curves for 6.2M126 are identical for the 90 m and 95 m version of the turbine.

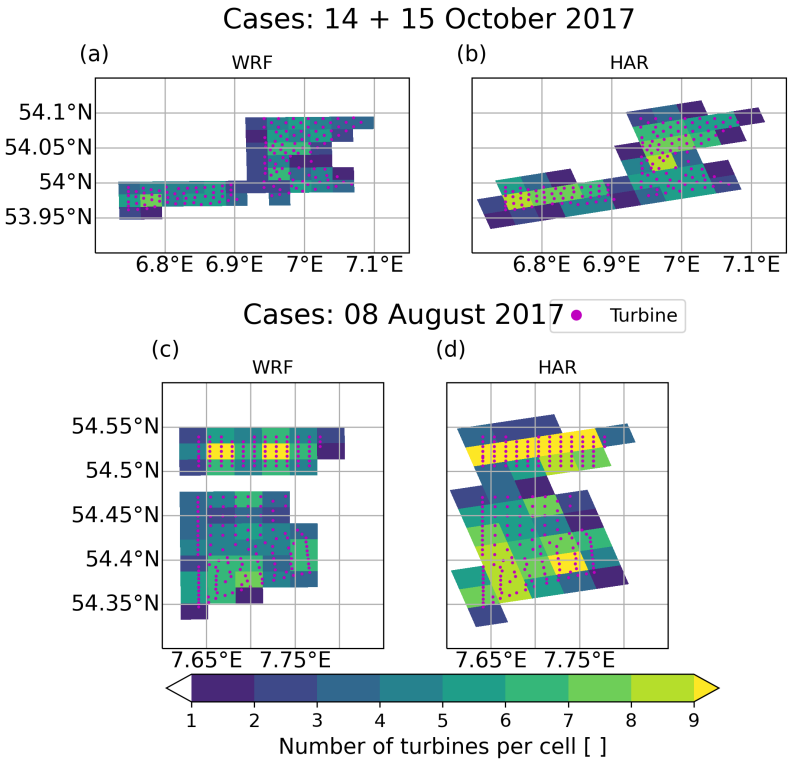

Figure 5. Number of turbines per grid cell in (a,c) WRF and (b,d) HARMONIE for (a,b) the wind farms relevant for case study 14. and 15 October 2017 and (c,d) the wind farms relevant for case study 08 August 2017.

we set the tuneable initial wake expansion coefficient, as introduced in Eq. 3, to f_r =1.7, as recommended in Volker et al. (2015) and used in other studies (Volker et al., 2017; Pryor et al., 2020). Previous studies (e.g. Volker et al., 2015; Larsén and

Fischereit, 2021) found that simulated wind speed deficits in the wake are not very sensitive to variation in f_r between 1.5 and 1.7. To confirm the low sensitivity within this range, we reproduced the case 15 October 2017 with f_r =1.5 and found only minor biases $< 0.1\text{ms}^{-1}$ close to the farm (not shown). Values for f_r outside the range of 1.5 and 1.7 were tested in Ali et al. (2023). They noted larger impacts for the tested values of 1.36 and 2.04 on wake length and wind speed deficit. However, a more detailed investigation of different f_r-values is beyond the scope of the current study, which focuses on existing best practices.

2.6 Evaluation metrics

To assess the agreement between observations and simulations, several error measures are used to evaluate the different components of the overall error: the bias (BIAS) assesses the systematic error, the standard deviation of errors (STDE) assesses the non-systematic error, and the root mean square error (RMSE) assesses the combined error. In addition, the correlation coefficient (CORR) is derived to assess the temporal agreement with the observations. CORR and STDE evaluate similar aspects of the model performance, but STDE is not dimensionless and therefore gives additional insights. The equations for the different error measures can be found, for example, in Schlünzen and Sokhi (2008). While two different models can perform the same in terms of one error measure, e.g. the same correlation coefficient, they might perform differently in terms of another error measure, e.g. different BIASes. Thus, having four different error measures has the advantage that different aspects of the performance can be evaluated. The error metrics are calculated for each transect and the median error over all transects is given in this manuscript.

Besides the agreement with measurements, the magnitude of the wind farm effect is evaluated. To characterize the magnitude, the difference between simulations with wind farms (FITCH / EWP) and simulations without wind farms (NWF) are calculated: FITCH-NWF and EWP-NWF for both WRF and HARMONIE. The correctness of the magnitude of the WFE cannot simply be assessed against the flight observations, since there are no observations without a WFE. To circumvent this problem, artificial observations without WFE ('obsNWF') are constructed based on a simple linear interpolation between two locations at either sides of the farm (or wake) on a flight transect. These artificial observations are shown exemplary as gray dash-dotted lines in Fig. 6. Since the background conditions also vary in time and space and the width of the wake increases with increasing distance from the farm, it is difficult to define which part of the track is already under wake influence and which part is not. Thus, two different locations are chosen to measure the uncertainty of the observational wake effect. The two locations are based on the location of the minimum and maximum WS value to the left of the farm (or wake) with respect to the mean wind direction (Fig. 6, left red crosses).

The presented method is very simplistic, but provides a way to quantify the wake effect in the observations. The method is similar to the method presented in Cañadillas et al. (2020), but instead of evaluating the maximal WFE, it provides the mean WFE. In addition, it also works for the case of measurements above the farm and for other variables other than WS. As a comparison, also the method by Cañadillas et al. (2020) is applied for the wake cases. Cañadillas et al. (2020) use an exponential function $U_R(x) = 1 - a \cdot \exp(-bx)$ for the wind speed recovery U_R as function of downstream distance x with coefficients a and b given in their study. The reference wind speed U_{ref} for each transect to calculate the maximum WFE

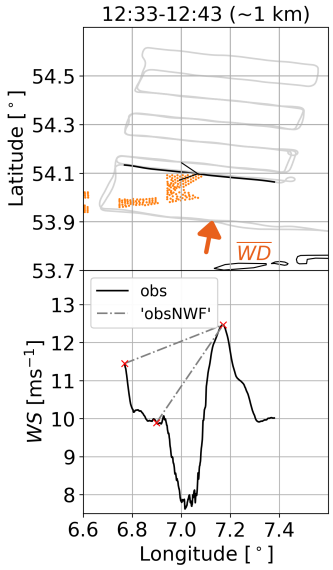

Figure 6. First row: Flight track (gray) with transect of interest (black) and turbines (orange); second row: wind speed (WS) for flight measurements (obs, black, solid) for the case 15 October 2017. Observational wake effects (obsNWF, gray) are as shown as dashed-dotted lines. Mean upwind transect wind direction ($\overline{WD}$, as in Table 2) is shown by the arrow. The title indicates the time of the transect and the median downstream distance from the farm.

at each x as $\mathrm{WFE}(x) = U_{ref}(x) - U_R(x) \cdot U_{ref}(x)$ is not provided in Cañadillas et al. (2020). Therefore, the reference wind speed is derived as mean over the three points of 'obsNWF' (Fig. 6, red crosses).

3 Results

3.1 Above a wind farm

3.1.1 Background conditions

In this case study, the simulations of WRF and HARMONIE with and without WFP are evaluated with WIPAFF aircraft measurements above the wind farm on 14 October 2017 (Table 2). During this case, the wind was from south-west (Table 2, Fig. 3), the atmosphere was stably stratified and low-level jets were present as discussed in detail in Siedersleben et al. (2020) and Larsén and Fischereit (2021). The prominent wind direction can also be seen in the wind farm wake direction visible in the 10 m winds from SAR and simulations (Fig. 7). HARMONIE winds simulated for 10 m height agree visually well with the SAR-derived winds, while WRF slightly overestimates the wind. Both models and both parameterizations, i.e. FITCH and EWP, visually capture extend of the farm wakes well compared to SAR.

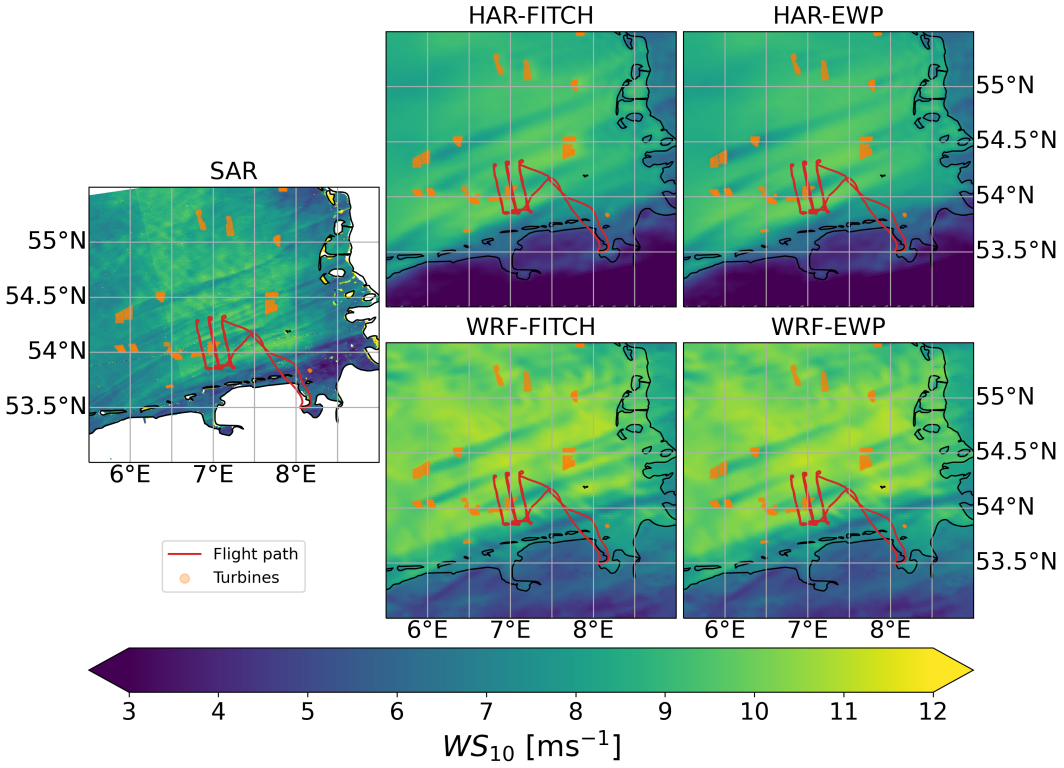

Figure 7. Wind speed at 10 m height from SAR on 14 October 2017 at 17:17, HARMONIE (HAR) with FITCH and EWP WFPs at 17:15 and WRF with FITCH and EWP WFPs at 17:20. The red lines are the flight path.

3.1.2 Transects above the farm

The measurement aircraft flew at a height of about 250 m six times above Gode Wind 1+2, as can be seen in the flight track in Fig. 8a,b (upper rows). The corresponding time is given in the title of the subfigures in Fig. 8. Although all transects were measured within 2 hours, wind speed varies quite considerably (Fig. 8a,b, center rows) by 1 ms^{-1}. Neither WRF nor HARMONIE can fully capture this temporal variability. ~~Although WRF overestimated the 10 m wind speed if compared to SAR (Fig. 7) , the~~ For the models, the two closest model output time steps (Table 1) to the transect times are shown to highlight the temporal variability of the conditions during the passing of the aircraft over the transect. Thus, for a good match between model and observations, the observations should be within the shaded area of the model output. Overall the wind speed at 250 m matches well with the observations for some transects~~as well as with HARMONIE~~, even though WRF overestimated the 10 m wind speed if compared to SAR (Fig. 7).

Above Gode Wind 1+2 WS is decreased and TKE increased (Fig. 8a,b, second and third rows) due to effect of the wind farm. Both WRF and HARMONIE equipped with the FITCH WFP (blue) can capture this effect. The EWP (red) can capture the wind speed reduction, but underestimates the magnitude of the reduction in both models. Furthermore, EWP does not

capture the increased magnitude of TKE above the farm. However, in contrast to the simulation without wind farms (NWF, yellow), EWP shows a reduced WS above the farm. Due to the relatively coarse resolution of 2 km in WRF and 2.5 km in HARMONIE, the speed-up on the side of the farm cannot be properly captured.

The wind direction, WD, is slightly off in HARMONIE (Fig. 8a,b bottom rows), especially in the earlier transects up to 15:50. A consequence is that the exact location of the wind speed deficit is not captured as well in HARMONIE as it is in WRF (Fig. 8a,b second rows).

3.1.3 Error statistics

The quantitative evaluation of the simulations against the flight measurements is difficult, since for some transects the background wind is not well simulated. This is visible on both sides of the farms, where HARMONIE and WRF overestimate WS (Fig. 8 second row). Since the thrust coefficient depends on wind speed (see SWT-6.0-154-curve in Fig. 4), the WFE differs for different background conditions. This is a common problem for evaluating WFPs as found in the review in Fischereit et al. (2022a).

In our case, the wind speed is within the range of 14 ms^{-1}–16 ms^{-1}, where the sensitivity of the thrust is already reduced compared to lower wind speeds, but still high (Fig. 4). To circumvent this problem, we calculate several error metrics that assess the different components of the overall error as described in Sect. 2.6. All error metrics are calculated for both WS and TKE, as well as for the two models with each 3 different scenarios, as shown in Sect. 2.5.

The statistics (Table 3) confirm that FITCH agrees best with the observations and that EWP performs reasonably well for WS, but as bad as NWF for TKE. Overall the error measures indicate comparable performance of WRF+WFP and HARMONIE+WFP, which indicates that the implementation of EWP was successful.

3.1.4 Wind farm effects

To evaluate the WFE above the farm (60 m above the rotor tip), the NWF scenario is subtracted from the simulations with wind farms as described in Sect. 2.6. Those differences are shown in Table 4. It shows that wind speed deficits at that height above the farm are around -0.75 ms^{-1} and TKE increase is around 0.5 $\mathrm{m}^2\mathrm{s}^{-2}$ according to the observations. However, there is some uncertainty in the artificially generated NWF observations. FITCH matches the magnitudes quite well, although it underestimates the mean TKE effect and slightly overestimates the WS effect. EWP slightly underestimates the WFE with respect to WS and has almost no WFE with respect to TKE.

Comparing the results for HARMONIE and WRF shows that the mean WFEs are slightly higher for HARMONIE compared to WRF for both FITCH and EWP (Table 4). There could be multiple reasons for this. Firstly, the different planetary boundary layer schemes applied in WRF and HARMONIE (Table 1). Secondly, the horizontal and vertical resolution differ between WRF and HARMONIE (Table 1) and consequently the wind turbines are differently assigned to the grid cells (Fig. 5).

Table 3. Median error metrics over all transects for 14 October 2017 for WRF (three left-most columns) and HARMONIE (three right-most columns) for three scenarios each: FITCH and EWP WFP and no-wind-farm (NWF) scenario. The error metrics bias (BIAS), standard deviation of errors (STDE), the root mean square error (RMSE) and the correlation coefficient are shown for both wind speed (WS) and turbulent kinetic energy (TKE). The cells are color coded row by row across all three case studies with respect to performance, with light color indicating best performance.

		WRF			HARMONIE		
		FITCH-obs	EWP-obs	NWF-obs	FITCH-obs	EWP-obs	NWF-obs
WS	BIAS [ms^{-1}]	0.54	1.07	1.40	0.72	1.17	1.69
	CORR	0.90	0.90	0.59	0.90	0.82	0.21
	RMSE [ms^{-1}]	0.62	1.21	1.63	0.88	1.27	1.87
	STDE [ms^{-1}]	0.40	0.53	0.83	0.43	0.51	0.88
TKE	BIAS [m^2 s^{-2}]	-0.11	-0.35	-0.36	-0.06	-0.34	-0.37
	CORR	0.84	-0.12	-0.24	0.86	-0.04	-0.23
	RMSE [m^2 s^{-2}]	0.32	0.62	0.62	0.29	0.64	0.66
	STDE [m^2 s^{-2}]	0.30	0.51	0.52	0.29	0.55	0.55

Table 4. Median wake effect over all transects for 14 October 2017 for WRF (two left-most columns), HARMONIE (two center columns) and observations (right-most column) for the difference of FITCH and no-wind-farm (NWF), EWP and NWF scenario and observations (obs) and artifically generated NWF-observations for both wind speed (WS) and turbulent kinetic energy (TKE).

	WRF		HARMONIE		Observations
	FITCH-NWF	EWP-NWF	FITCH-NWF	EWP-NWF	obs-obsNWF
WS [ms^{-1}]	-0.91	-0.38	-1.01	-0.56	-0.73±0.10
TKE [m^2 s^{-2}]	0.26	0.01	0.32	0.02	0.54±0.00

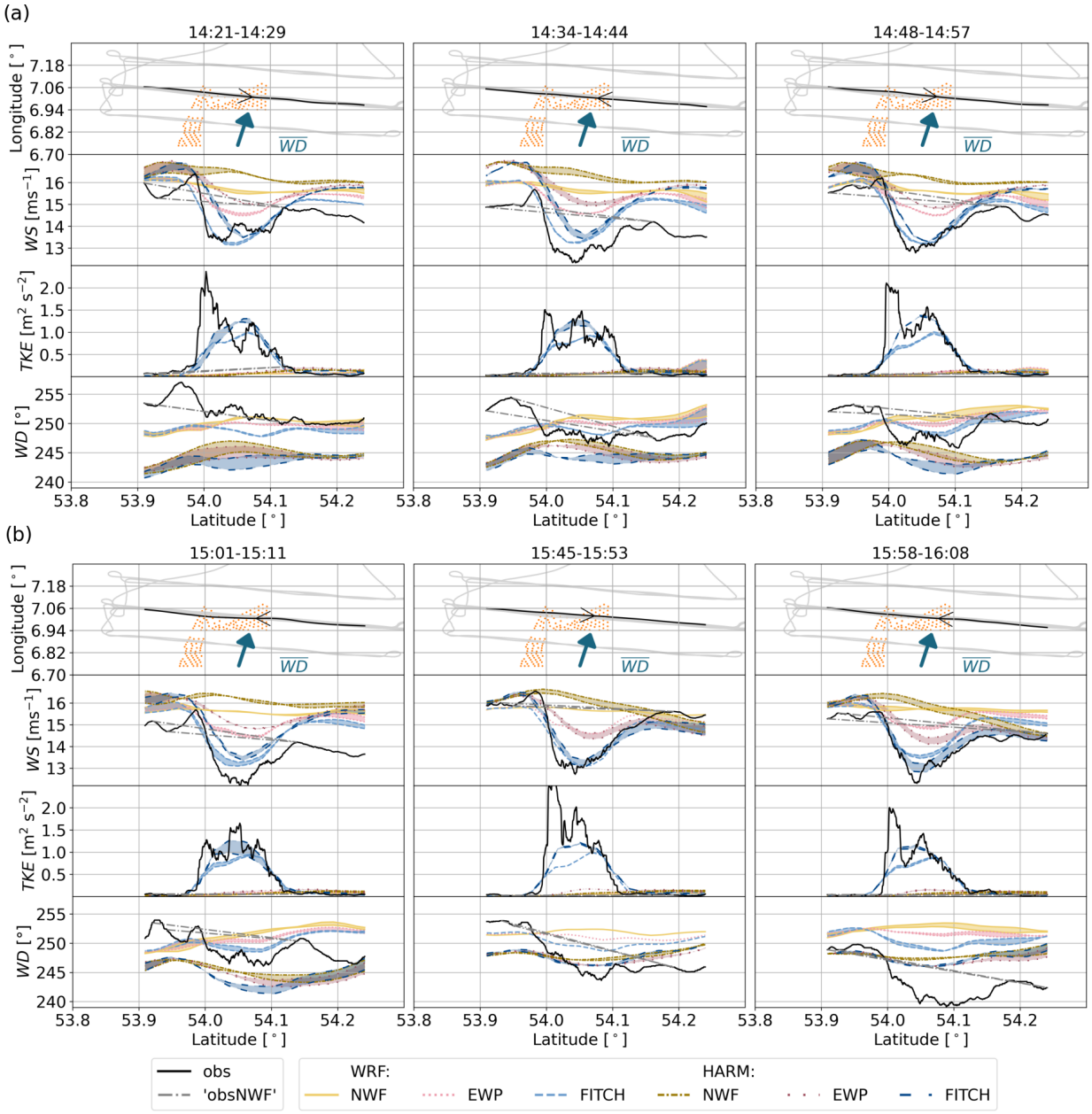

Figure 8. Transects for case study on 14 October 2017 for (a) earlier transects and (b) later transects. First row: Flight track (gray) with transect of interest (black) and turbines (orange) and mean upwind transect wind direction ($\overline{WD}$, as in Table 2) as arrow with respect to flight track; second row: wind speed (WS); third row: turbulent kinetic energy (TKE); fourth row: wind direction (WD) for flight measurements (black), WRF simulations (brighter colours, densely broken lines) and HARMONIE simulations (darker colours, loosely broken lines) for the no-wind-farm scenario (NWF, yellow, solid and dashed dotted lines), EWP parameterization (red, dotted lines) and FITCH parameterization (blue, dashed lines) are shown for the median flight height of each transect (around 250 m). For each simulation two lines for the nearest model output time steps with shaded area between them are shown. Observational wake effects (obsNWF) are as shown as gray dashed-dotted lines (Sect. 2.6). The title of each column corresponds to the time of the respective transect.

3.2 In the wake of a wind farm

To evaluate the performance of the model in the wake of the wind farm at around hub height, we look at two case studies: 15 October 2017 and 08 August 2017. The case 15 October 2017 is chosen because the background meteorology was better matched from the simulations due to a less complex meteorological situation. The case 08 August 2017 is chosen because an effect on the temperature of the wind farm was observed, which is interesting to consider from a NWP point of view, which does not focus solely on power forecast.

3.2.1 Background conditions

On 15 October 2017 around the flight time wind was coming from the southern coast of the German Bight. The aircraft was flying at about 120 m height in the wake of Nordsee One and Gode Wind 1+2. The atmosphere was slightly stable stratified (Cañadillas et al., 2020). Compared to SAR, both HARMONIE and WRF overestimate the 10 m wind speed, but show the same gradient of increasing wind towards the North (Fig. 9).

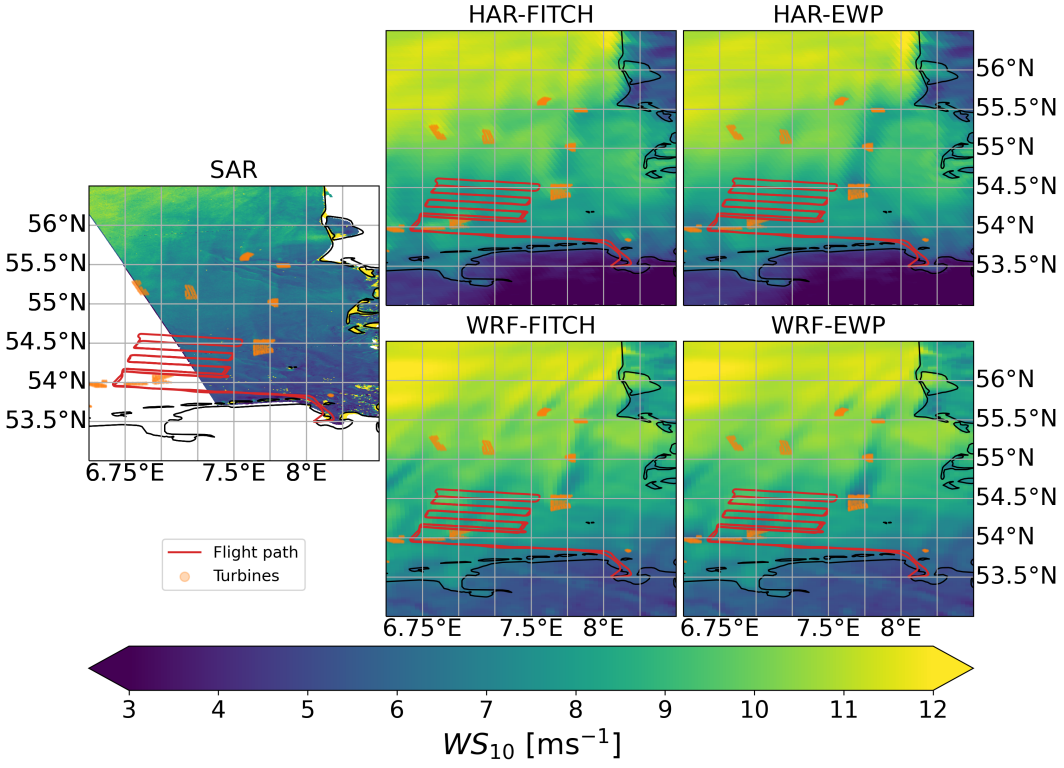

Figure 9. Same as Fig. 7, but for 15 October 2017 and for WRF at 17:10, HAR at 17:15, SAR at 17:09.

The meteorological situation on 08 August 2017 is much more dynamic with patches of high and low wind speeds (Fig. 10), but it is also classified as slightly stable in Cañadillas et al. (2020). The models can capture this general behaviour, but do not correctly simulate the location of these patches in the 10 m wind with respect to SAR (Fig. 10).

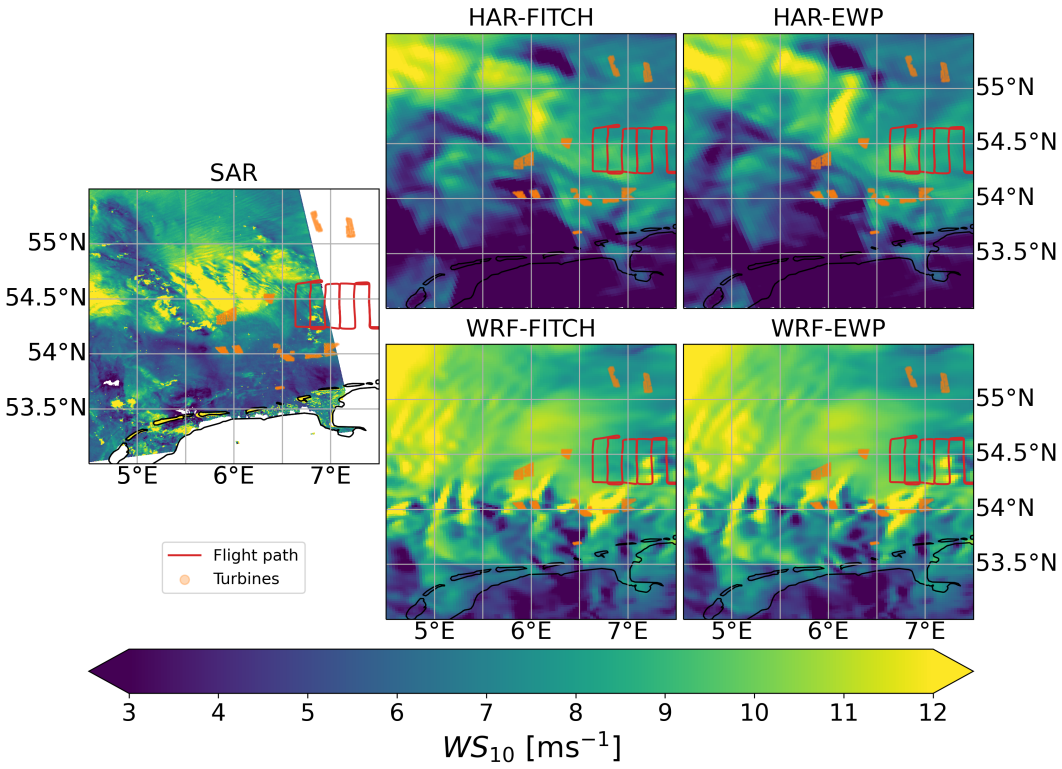

Figure 10. Same as Fig. 7, but for 08 August 2017 and for WRF at 17:20, HAR at 17:30, SAR at 17:25.

3.2.2 Transects in the wake

While the wind speed at 10 m was overestimated by the simulations with respect to SAR for 15 October 2017 (Fig. 9), the wind speed at the transects at 120 m height is quite well matched (Fig. 11a,b second rows). In the sequence of transects, a wind speed reduction in the wake downstream of GodeWind 1+2 and with a smaller amplitude also for Nordsee One is visible in the transects from 12:35 onward compared to the transect upstream of the farms at 12:25. The magnitude of the wake deficit gradually decreases with increasing distance from the farm.

TKE is increased downstream of the farm (Fig. 11a,b, third rows), especially near the farm. The TKE increase diminishes faster with increasing distance from the farm than the WS decrease and is only visible through two peaks around 19 km behind the farm (transect at 13:15). High TKE values are visible especially at the edges of the wake as indicated by the "M"-shape

around the wake (e.g. Fig. 11, third row, for 13:05 onward). This increased turbulence is generated by the shear in that region due to the gradient in wind speed inside and outside of the wake. This was also described in Platis et al. (2020).

Both HARMONIE and WRF agree quite well with the observations ahead of the farm and for some flight legs. The wind direction is slightly more westerly in WRF, which causes a slight displacement of the maximum wind speed deficit at e.g. 30 km (13:25-13:35). Both EWP and FITCH in both models can capture the wake deficit. However, EWP underestimates the magnitude of the wind speed deficit and also strongly underestimates the increase in TKE in the wake. HARMONIE-FITCH best captures the magnitude of the TKE increase just downwind of the farm. WRF-FITCH produces slightly smaller magnitudes, although both use a TKE factor of 1. Neither of the models can capture the "M"-Shaped behaviour of the TKE distribution further downstream the wake. This is expected from the coarse resolution of the mesoscale models.

Fig. 11b only shows the transects up to about 30 km downstream (13:35), since for increasing distance, the performance of especially WRF deteriorates due to the increasing offset in the simulated wind direction. As the main objective is to evaluate the performance of the WFP in HARMONIE and WRF and not the background physics, the figure for the later transects is placed in the Appendix (Fig. A1). At these transects, the trend of increasing wake recovery and decreasing effects on TKE continues, and later closer transects (at 15:05) are again better captured.

For 08 August 2017 the respective figure showing the transects is placed in the appendix (Fig. A2), because the general trends of the results are quite similar to those for 15 October 2017: The magnitudes of the wind speed deficit and the TKE enhancement agree better for FITCH than for EWP. Both EWP and FITCH capture the gap between the two farms.

3.2.3 Error statistics

We calculate error metrics as described in Sect. 2.6 to quantify the agreement for the different scenarios with observations for the transects highlighted in Fig. 11 and Fig. A2. As for the case above the farm, overall HARMONIE and WRF perform similarly (Table 5, Table 6) and again the FITCH agrees best with the observations, indicated by high correlation coefficients and low BIASes for 15 October 2017. For 08 August 2017, the FITCH simulations show large BIASes for WS (Table 6) and better performance of EWP. This is due to a systematic underestimation of the wind speed compared to the observations, which is amplified in FITCH and is highlighted by the BIAS. However, looking at the correlation and STDE as a non-systematic error metric indicates that FITCH also outperforms EWP in this case. This again highlights the challenge of simulating background meteorology correctly. For TKE FITCH performs best in terms of all error measures.

For Table 5 and Table 6 the mean over all transects is taken. Since this also includes transects with very small TKE-related WFE 20 km and more downstream (Fig. 11b, Fig. A2b), the difference between EWP and FITCH in the error measures is not that pronounced except for the correlation. This indicates that although EWP greatly underestimates TKE close to the farm, further downstream at hub height this underestimation is of minor importance due to the diminishing effects for wind farm generated TKE.

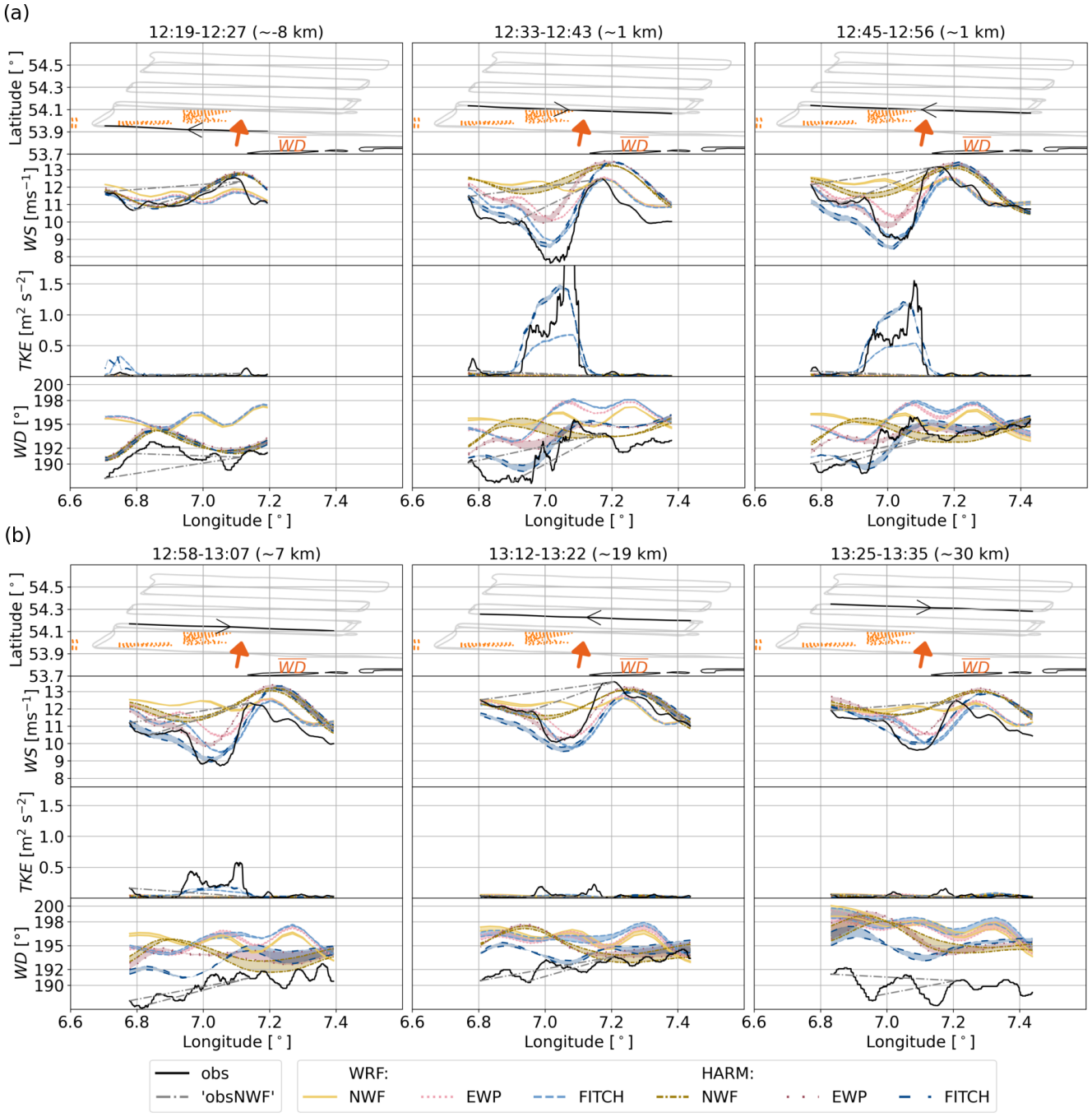

Figure 11. As Fig. 8, but for 15 October 2017 and for around 120 m height. The title in each column indicates the time of the transect and the median downstream distance from the farm.

Table 5. As Table 3, but for case 15 October 2017.

		WRF			HARMONIE		
		FITCH-obs	EWP-obs	NWF-obs	FITCH-obs	EWP-obs	NWF-obs
WS	BIAS [ms^{-1}]	0.07	0.36	0.79	0.29	0.71	1.06
	CORR	0.80	0.81	0.13	0.79	0.85	0.67
	RMSE [ms^{-1}]	0.68	0.67	1.27	0.86	0.92	1.29
	STDE [ms^{-1}]	0.51	0.58	1.01	0.72	0.53	0.67
TKE	BIAS [m^2 s^{-2}]	-0.03	-0.05	-0.05	-0.01	-0.07	-0.07
	CORR	0.49	-0.31	-0.27	0.46	-0.24	-0.15
	RMSE [m^2 s^{-2}]	0.10	0.11	0.11	0.09	0.12	0.12
	STDE [m^2 s^{-2}]	0.10	0.10	0.10	0.08	0.10	0.10

Table 6. As Table 3, but for case 08 August 2017.

		WRF			HARMONIE		
		FITCH-obs	EWP-obs	NWF-obs	FITCH-obs	EWP-obs	NWF-obs
WS	BIAS [ms^{-1}]	-2.27	-1.66	-0.79	-1.81	-1.16	-0.58
	CORR	0.69	0.55	-0.06	0.82	0.74	0.07
	RMSE [ms^{-1}]	2.46	2.01	1.59	1.99	1.51	1.42
	STDE [ms^{-1}]	1.00	1.03	1.38	0.81	0.84	1.31
TKE	BIAS [m^2 s^{-2}]	-0.21	-0.25	-0.26	-0.08	-0.28	-0.28
	CORR	0.79	0.27	-0.31	0.74	-0.07	-0.47
	RMSE [m^2 s^{-2}]	0.28	0.33	0.34	0.18	0.36	0.36
	STDE [m^2 s^{-2}]	0.19	0.21	0.22	0.15	0.22	0.22

3.2.4 Wind farm effects

The magnitude of the WFEs is derived again by the difference between the simulations with and without WFP. By calculating the mean difference across each transect, the magnitude of the WFE is derived with increasing distance from the farm for simulations and observations (Fig. 12). For the observations the methods described in Sect. 2.6 are used to generate an artificial NWF-observation. Note that the method by Cañadillas et al. (2020) can only be applied to WS and not to TKE.

Both cases show that TKE (Fig. 12, dotted lines above zero) recovers faster to background levels compared to WS (Fig. 12, solid lines) behind the farm at hub height: after 20-30 km downstream almost no mean TKE effect along the transect is detectable, while wind speed is still reduced compared to the NWF scenario. The wind speed deficit is stronger on 08 August 2017 than on 15 October 2017, but recovery is also faster, as indicated by the steeper lines. This is also confirmed by the

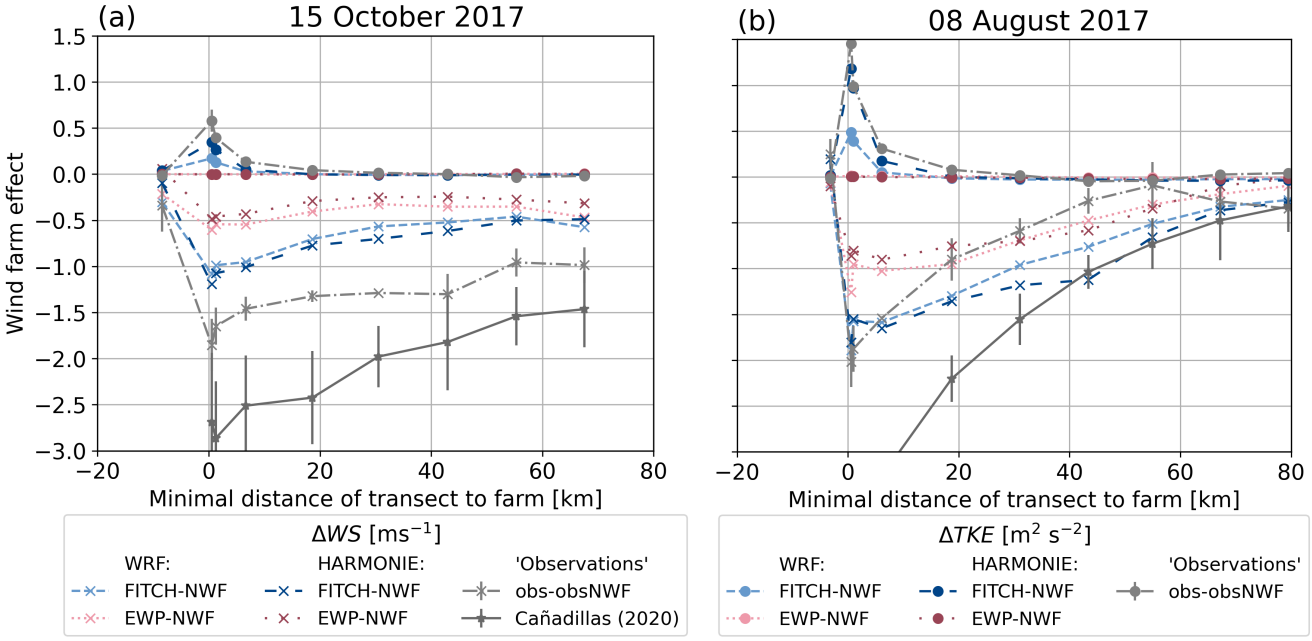

Figure 12. Wake effect at around hub height defined as scenario with WFP (FITCH and EWP) minus scenario without wind farm (NWF) in terms of WS reduction in ms^{-1} (lines with crosses) and TKE increase in m^2s^{-2} (lines with circles) for different transects with a certain minimal distance to the farm for WRF and HARMONIE with same color and line style coding as in Fig. 8 for (a) 15 October 2017 and (b) 08 August 2017. Observational wake effects have been derived based on the methods described in Sect. 2.6. The unbiased standard error of the mean is used to draw the error bars around the observational wake effect.

artificially derived observational WFE and by the exponential function provided by Cañadillas et al. (2020). The WFE based on Cañadillas et al. (2020) are stronger, since they represent the maximal WFE, in contrast to the mean WFE in our study.

The WFEs in WRF and HARMONIE are comparable for the two WFPs with slightly higher values for HARMONIE-FITCH than for WRF-FITCH and slightly higher values for WRF-EWP than for HARMONIE-EWP. The similarity confirms the conclusions in Sect. 3.1.4 that the implementations of FITCH and EWP in HARMONIE have been successful.

3.2.5 Impact on temperature and humidity

On 08 August 2017 a slight cooling (less than 0.5 K) and humidification (less than 0.5 hPa) was observed in the wake of the farm at hub height a few kilometers downstream of the farm (Fig. 13, compare first with the second and third columns). This WFE is superimposed by a general cooling and humidifying trend as moving further offshore. On the transects 6 km and further downstream this effect is difficult to detect, since it is super-imposed by the variability in the background conditions. Both HARMONIE and WRF only match the background conditions well for some transects. Therefore, it is difficult to compare the effect quantitatively. However, at least for WRF, of the three scenarios, EWP best captures this effect, since it shows the largest temperature drop and humidity increase compared to the other scenarios. In HARMONIE the transects upwind of the

farm already differ greatly for the different scenarios; thus it is difficult to conclude whether the WFPs capture this effect. Therefore, only WRF will be used for a more detailed analysis in the following.

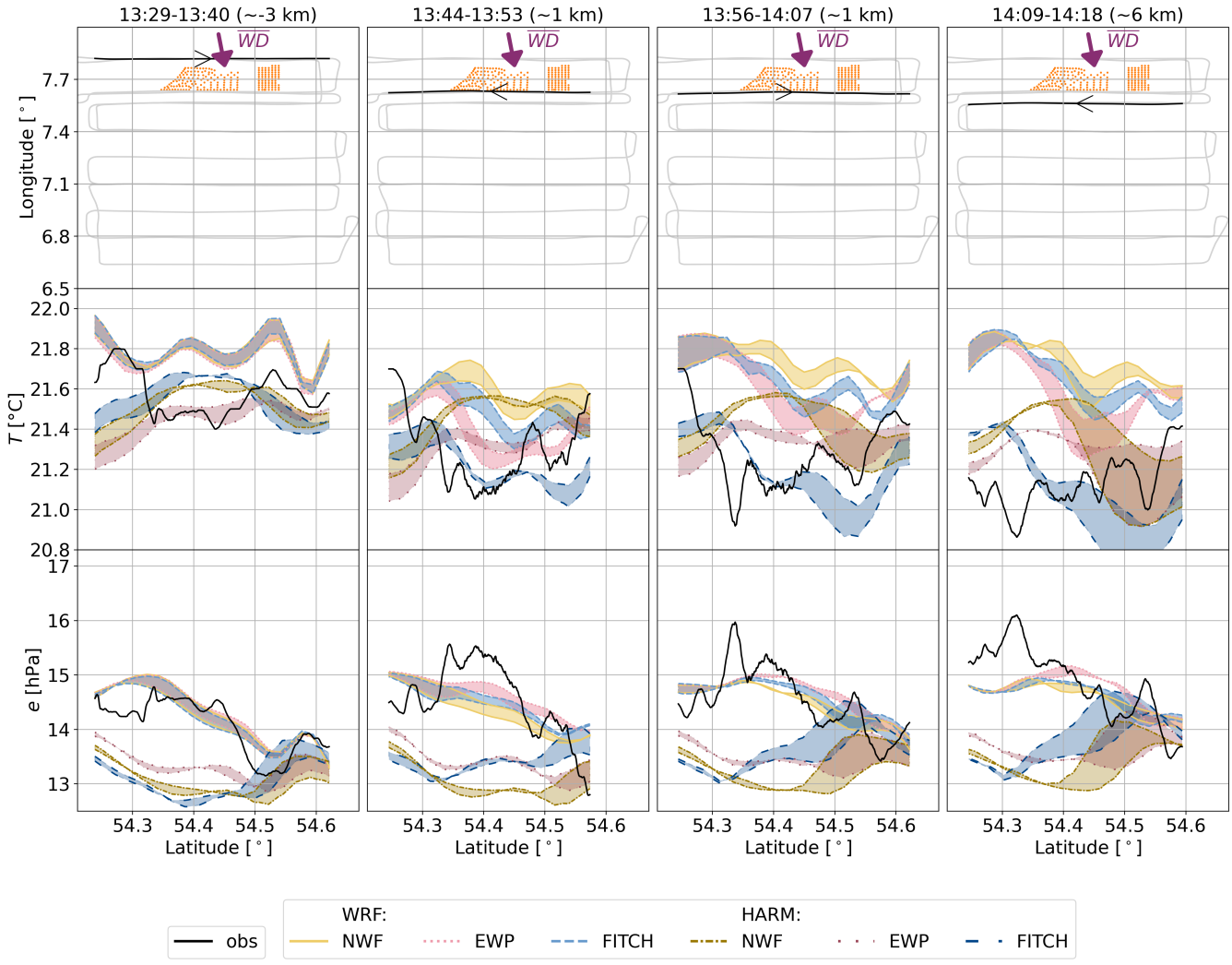

Figure 13. As Fig. 8, but for 08 August 2017 and around 90 m height and for (center row) temperature, (last row) vapour pressure.

The profiles in Fig. 14 show the reason for this WFE. The yellow NWF scenario indicates how profiles evolve with increasing distance from the shore: the inversion moves upward, the air cools and humidifies, and wind speed and TKE increase. These changes happen throughout the lower atmosphere, e.g. also close to the surface.

Due to the presence of wind farm effects in EWP and FITCH the evolution of these profiles is modified. Compared to NWF, in EWP the inversion height is increased and reaches the upper part of the rotor. This results in lower temperatures and higher vapour pressure at hub height. The weak low-level jet present in NWF is removed through the introduced wind speed deficit

from the turbines (Fig. 14d) and TKE levels close to the ground are reduced in EWP compared to NWF. Similarly, temperature, humidity, and wind speed are modified close to the ground, indicating that also the surface fluxes have changed. It is difficult to quantify this effect, however, due to the evolving profile with distance from the shore in the NWF case, as discussed above.

In contrast to EWP, the strong mixing in FITCH (Fig. 14c) leads to lower inversion height compared to NWF, which is even moved below hub height (Fig. 14a). This causes the cooling that is also visible in FITCH compared to NWF at hub height in the transects in Fig. 13.

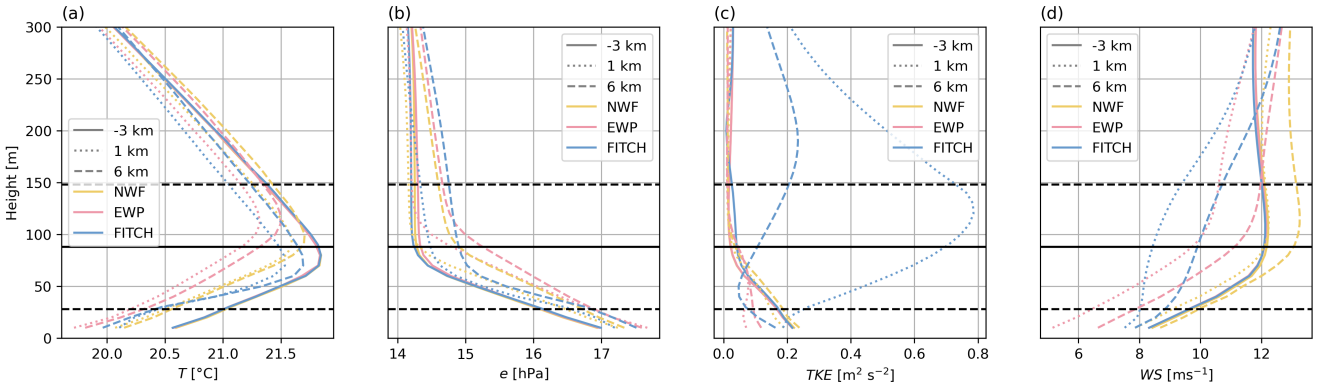

Figure 14. Profiles at the transects in Fig. 13 for (a) temperature, (b) vapour pressure, (c) turbulent kinetic energy and (d) wind speed at different distances from the farm (line style) at Latitude 54.4°. All results are for WRF for NWF (yellow), EWP (red) and FITCH (blue).

4 Discussion

The main goal of this study was to derive, how well the implemented WFPs agree in WRF and HARMONIE to evaluate the implementation of the WFPs in HARMONIE. Therefore, the setups of WRF and HARMONIE follow best practices for standard use of the two models, respectively (Table 1). Thus, we applied HARMONIE in forecast mode and WRF in hindcast mode, which is a common setup for wind energy research. Since a control simulation without wind farms was conducted both for WRF and HARMONIE, the main goal could be reached even with the different setups. However, we acknowledge that due to the different resolution and grids, wind turbines have been assigned to different grid cells (Fig. 5) in WRF and HARMONIE. This influences the direct comparison between WRF and HARMONIE. In addition, the different grids in WRF and HARMONIE could also affect the modelling of the background meteorology, which has implications for comparison against real measurements as discussed below. It is difficult to isolate and quantify the effects of the different grids directly, since also the physics schemes as well as the initial and boundary data ~~differs~~ differ between WRF and HARMONIE (Table 1). More idealized test cases and setups with WRF and HARMONIE could be used in the future to compare WRF and HARMONIE directly and isolate some effects, such as differences in the grids and in the physics schemes.

The control simulation without wind farms (NWF) for WRF and HARMONIE was used to derive the magnitude of the wind farm effects both for WS and TKE as bias compared to a simulation with WFP. To compare these magnitudes with the research flight measurements, an artificial observation without wind farms was created by simple linear interpolation between two points outside the farm wake. However, there is some uncertainty in how to define whether a location is outside the farm wake while still being close enough to not be influenced by other meteorological background effects. This exhibits uncertainty that was captured by using different artificially produced observations without wind farm effects. However, as indicated by the NWF simulation, there was considerably variability in the background wind speed within the farm area. Thus, a linear interpolation can only provide a rough estimate of the magnitude of the wake effect in the observations.

The evaluation of the WFP against real measurements is challenging, since the models ability of simulating the background meteorological conditions influences the calculations of the WFP: The thrust coefficient depends non-linearly on the wind speed (Fig. 4) and thus different background conditions will result in different WFEs. Standard operational verification of HARMONIE includes mostly observations from automatic weather stations close to the surface. Some evaluation has also been done for masts (Kangas et al., 2016), but further evaluation of the forecasts from HARMONIE in heights relevant to wind energy are needed. This evaluation should also include masts undisturbed by wind farms to be able to evaluate the forecast skill at heights of up to 250 m.

5 Conclusions

Wind farm effects are increasingly important to consider in Numerical Weather Prediction (NWP) models. In this study, we implemented the Explicit Wake Parameterization (EWP, Volker et al., 2015) in the nonhydrostatic NWP model HARMONIE. The newly implemented EWP scheme, as well as the already implemented (van Stratum et al., 2022) WFP by Fitch et al. (2012) (FITCH), were evaluated against research flight measurements taken from the project WIPAFF (Bärfuss et al., 2019) as well as against model simulations with the NWP model WRF, which has been frequently used before to evaluate wind farm effects (Fischereit et al., 2022a).

The results show that the implementations of EWP and FITCH are successful and that, of the two WFPs, FITCH agrees in general better with measurements, especially for TKE. Most note-worthy is the underestimation of TKE by EWP close to the farm, which has also been reported previously (Larsén and Fischereit, 2021). The high values of TKE decrease fast with increasing distance of the farm, leaving an "M"-shape pattern with high TKE values close to the edge of the wake. Due to this fast decrease, the underestimation of TKE by EWP is of minor importance further downstream. Nevertheless, this study indicates that taking only the implicit TKE formation due to vertical shear into account is not sufficient. Instead, an explicit source of TKE is required to consider the TKE formation from the rotational motion of the rotor as well as from tip vortices. Furthermore, this study showed that EWP also exhibits a different wake recovery at hub height as well as a different vertical wake profile of TKE, wind speed and other parameters. The reasons for these differences are both the vertical wake expansion considered in EWP as well as the missing explicit TKE source. However, observations of the vertical profile in the wake were

not available for comparison and thus further studies are necessary to investigate the correct shape of the profile in the wake. Nevertheless, according to this study, EWP shows possibilities of improvement that will be addressed in future work.

As the next step, forecasts with all wind turbines, both onshore and offshore, within the Northern Europe DMI domain will be performed for longer periods. This allows to estimate the full impact of currently installed wind turbines on weather and weather forecasting. The established wind turbine data base as well as the results will be presented in part 2 of this series (Fischereit et al., 2023a).

Code and data availability. The ALADIN and HIRLAM consortia cooperate on the development of a shared system of model codes. The HARMONIE-AROME model configuration forms part of this shared ALADIN-HIRLAM system. According to the ALADIN-HIRLAM collaboration agreement, all members of the ALADIN and HIRLAM consortia are allowed to license the shared ALADIN-HIRLAM codes to nonanonymous requests within their home country for noncommercial research. Access to the full HARMONIE-AROME codes can be obtained by contacting one of the member institutes of the HIRLAM consortium (see https://hirlam.github.io/HarmonieSystemDocumentation). The code-changes to enable wind farms in HARMONIE-AROME are made available in the supplement material.

The WRF model is available from https://github.com/wrf-model/WRF. Modifications to WRF for EWP are available in the supplement material. Updates to EWP will be made available in the future at https://gitlab.windenergy.dtu.dk/WRF/EWP.

The flight measurements are available from Bärfuss et al. (2019). The SAR data is available from https://science.globalwindatlas.info/ (Badger et al., 2022). ERA5 data is available from Hersbach et al. (2018) and the OSTIA data is available from http://my.cmems-du.eu/motu-web/Motu.

The wind farm input data as well as the namelists for WRF are permanently archived at Fischereit et al. (2023b) along with the scripts to reproduce the tables and figures in this manuscript.

Appendix A

Author contributions. JF implemented the EWP parameteriztion with the help of NT and HV. JF designed the experiments, performed the simulations and analysed the results. XG post-processed the flight measurements. GG and EK acquired funding for this research. JF prepared the manuscript with contributions from XG and HV. All coauthors discussed the analysis, reviewed and edited the manuscript.

Competing interests. The authors declare no competing interests.

Disclaimer. TEXT

Acknowledgements. Part of the funding is by the Danish state through the National Centre for Climate Research (NCKF). We are grateful for the open access measurements in Bärfuss et al. (2019) from the project WIPAFF (wind park far field). We would like to thank the members of the NWP group at DMI for their helpful advice on running HARMONIE. Data processing and visualization for this study was in part conducted using the python programming language and involved use of the following software packages: NumPy (van der Walt et al., 2011), pandas (McKinney, 2010), xarray (Hoyer and Hamman, 2017), Matplotlib (Hunter, 2007) and Cartopy (Met Office, 2015). We thank the open-source community for the tools provided. The color scheme for some figures are taken from Paul Tol's notes (https://personal.sron.nl/~pault/, last accessed: 31.05.2023)

References

Ali, K., Schultz, D. M., Revell, A., Stallard, T., and Ouro, P.: Assessment of Five Wind-Farm Parameterizations in the Weather Research and Forecasting Model: A Case Study of Wind Farms in the North Sea, Monthly Weather Review, 151, 2333–2359, https://doi.org/10.1175/MWR-D-23-0006.1, 2023.

Archer, C. L., Wu, S., Ma, Y., and Jiménez, P. A.: Two Corrections for Turbulent Kinetic Energy Generated by Wind Farms in the WRF Model, Monthly Weather Review, 148, 4823–4835, https://doi.org/10.1175/MWR-D-20-0097.1, 2020.

Badger, M., Karagali, I., and Cavar, D.: Offshore wind fields in near-real-time, https://doi.org/10.11583/DTU.19704883.v1, 2022.

Baidya Roy, S. and Traiteur, J. J.: Impacts of wind farms on surface air temperatures, Proc National Academy of Sci, 107, 17 899–17 904, https://doi.org/10.1073/pnas.1000493107, 2010.

Bärfuss, K., Hankers, R., Bitter, M., Feuerle, T., Schulz, H., Rausch, T., Platis, A., Bange, J., and Lampert, A.: In-situ airborne measurements of atmospheric and sea surface parameters related to offshore wind parks in the German Bight, https://doi.org/10.1594/PANGAEA.902845, 2019.

Bénard, P., Vivoda, J., Masˇek, J., Smolíková, P., Yessad, K., Smith, C., Brozˇková, R., and Geleyn, J.-F.: Dynamical kernel of the Aladin-NH spectral limited-area model: Revised formulation and sensitivity experiments, Quarterly Journal of the Royal Meteorological Society, 136, 155–169, https://doi.org/10.1002/qj.522, 2010.

Bengtsson, L., Andrae, U., Aspelien, T., Batrak, Y., Calvo, J., de Rooy, W., Gleeson, E., Hansen-Sass, B., Homleid, M., Hortal, M., Ivarsson, K.-I., Lenderink, G., Niemelä, S., Nielsen, K. P., Onvlee, J., Rontu, L., Samuelsson, P., Muñoz, D. S., Subias, A., Tijm, S., Toll, V., Yang, X., and Køltzow, M. Ø.: The HARMONIE–AROME Model Configuration in the ALADIN–HIRLAM NWP System, Monthly Weather Review, 145, 1919–1935, https://doi.org/10.1175/MWR-D-16-0417.1, 2017.

Bouteloup, Y., Seity, Y., and Bazile, E.: Description of the sedimentation scheme used operationally in all Météo-France NWP models, Tellus A: Dynamic Meteorology and Oceanography, 63, 300, https://doi.org/10.1111/j.1600-0870.2010.00484.x, 2011.

Cañadillas, B., Foreman, R., Barth, V., Siedersleben, S., Lampert, A., Platis, A., Djath, B., Schulz-Stellenfleth, J., Bange, J., Emeis, S., and Neumann, T.: Offshore wind farm wake recovery: Airborne measurements and its representation in engineering models, Wind Energy, 23, 1249–1265, https://doi.org/10.1002/we.2484, 2020.

Danielson, J. J. and Gesch, D. B.: Global multi-resolution terrain elevation data 2010 (GMTED2010), Tech. rep., Earth Resources Observation and Science (EROS) Center, 2011.

de Rooy, W. C. and Pier Siebesma, A.: Analytical expressions for entrainment and detrainment in cumulus convection, Quarterly Journal of the Royal Meteorological Society, 136, 1216–1227, https://doi.org/10.1002/qj.640, 2010.

de Rooy, W. C. and Siebesma, A. P.: A Simple Parameterization for Detrainment in Shallow Cumulus, Monthly Weather Review, 136, 560–576, https://doi.org/10.1175/2007MWR2201.1, 2008.

de Rooy, W. C., Siebesma, P., Baas, P., Lenderink, G., de Roode, S. R., de Vries, H., van Meijgaard, E., Meirink, J. F., Tijm, S., and van 't Veen, B.: Model development in practice: a comprehensive update to the boundary layer schemes in HARMONIE-AROME cycle 40, Geoscientific Model Development, 15, 1513–1543, https://doi.org/10.5194/gmd-15-1513-2022, 2022.

Donlon, C. J., Martin, M., Stark, J., Roberts-Jones, J., Fiedler, E., and Wimmer, W.: The Operational Sea Surface Temperature and Sea Ice Analysis (OSTIA) system, Remote Sensing of Environment, 116, 140–158, https://doi.org/10.1016/j.rse.2010.10.017, 2012.

Fischereit, J., Brown, R., Guo Larsén, X., Badger, J., and Hawkes, G.: Review of Mesoscale Wind-Farm Parametrizations and Their Applications, Boundary-Layer Meteorology, 182, 175–224, https://doi.org/10.1007/s10546-021-00652-y, 2022a.

Fischereit, J., Schaldemose Hansen, K., Larsén, X. G., van der Laan, M. P., Réthoré, P.-E., and Murcia Leon, J. P.: Comparing and validating intra-farm and farm-to-farm wakes across different mesoscale and high-resolution wake models, Wind Energy Science, 7, 1069–1091, https://doi.org/10.5194/wes-7-1069-2022, 2022b.

Fischereit, J., Olsen, B. T., Imberger, M., Vedel, H., Larsén, X. G., Hahmann, A. N., Giebel, G., and Kaas, E.: Modelling wind farm effects in HARMONIE-AROME (cycle 43.2.2) – part 2: Application to Europe, Geoscientific Model development, to be submitted, 2023a.

Fischereit, J., Vedel, H., Larsén, X. G., Theeuwes, N. E., Giebel, G., and Kaas, E.: Documentation for Modelling wind farm effects in HARMONIE-AROME, https://doi.org/10.5281/ZENODO.7759987, 2023b.

Fitch, A. C., Olson, J. B., Lundquist, J. K., Dudhia, J., Gupta, A. K., Michalakes, J., and Barstad, I.: Local and Mesoscale Impacts of Wind Farms as Parameterized in a Mesoscale NWP Model, Mon Weather Rev, 140, 3017–3038, https://doi.org/10.1175/MWR-D-11-00352.1, 2012.

Hersbach, H., Bell, B., Berrisford, P., Biavati, G., Horányi, A., Muñoz Sabater, J., Nicolas, J., Peubey, C., Radu, R., Rozum, I., Schepers, D., Simmons, A., Soci, C., Dee, D., and Thépaut, J.-N.: ERA5 hourly data on single levels from 1979 to present, Copernicus Climate Change Service (C3S) Climate Data Store (CDS), Accessed o, https://doi.org/10.24381/cds.adbb2d47, 2018.

Hoyer, S. and Hamman, J. J.: xarray: N-D labeled Arrays and Datasets in Python, Journal of Open Research Software, 5, https://doi.org/10.5334/jors.148, 2017.

Hunter, J. D.: Matplotlib: A 2D Graphics Environment, Computing in Science \& Engineering, 9, 90–95, https://doi.org/10.1109/MCSE.2007.55, 2007.

Iacono, M. J., Delamere, J. S., Mlawer, E. J., Shephard, M. W., Clough, S. A., and Collins, W. D.: Radiative forcing by long-lived greenhouse gases: Calculations with the AER radiative transfer models, Journal of Geophysical Research, 113, D13 103, https://doi.org/10.1029/2008JD009944, 2008.

IRENA: FUTURE OF WIND Deployment, investment, technology, grid integration and socio-economic aspects, Tech. rep., \url{https://www.irena.org/-/media/Files/IRENA/Agency/Publication/2019/Oct/IRENA_Future_of_wind_2019.pdf}, last accessed: 22.03.2021, https://www.irena.org/-/media/Files/IRENA/Agency/Publication/2019/Oct/IRENA_Future_of_wind_2019.pdf, 2019.

Kain, J. S.: The Kain–Fritsch Convective Parameterization: An Update, Journal of Applied Meteorology, 43, 170–181, https://doi.org/10.1175/1520-0450(2004)043<0170:TKCPAU>2.0.CO;2, 2004.

Kangas, M., Rontu, L., Fortelius, C., Aurela, M., and Poikonen, A.: Weather model verification using Sodankylä mast measurements, Geoscientific Instrumentation, Methods and Data Systems, 5, 75–84, https://doi.org/10.5194/gi-5-75-2016, 2016.

Larsén, X. G. and Fischereit, J.: A case study of wind farm effects using two wake parameterizations in the Weather Research and Forecasting (WRF) model (V3.7.1) in the presence of low-level jets, Geoscientific Model Development, 14, 3141–3158, https://doi.org/10.5194/gmd-14-3141-2021, 2021.

Lascaux, F., Richard, E., and Pinty, J.-P.: Numerical simulations of three different MAP IOPs and the associated microphysical processes, Quarterly Journal of the Royal Meteorological Society, 132, 1907–1926, https://doi.org/10.1256/qj.05.197, 2006.

Lenderink, G. and Holtslag, A. A.: An updated length-scale formulation for turbulent mixing in clear and cloudy boundary layers, Quarterly Journal of the Royal Meteorological Society, 130 C, 3405–3427, https://doi.org/10.1256/qj.03.117, 2004.

Masson, V., Le Moigne, P., Martin, E., Faroux, S., Alias, A., Alkama, R., Belamari, S., Barbu, A., Boone, A., Bouyssel, F., Brousseau, P., Brun, E., Calvet, J.-C., Carrer, D., Decharme, B., Delire, C., Donier, S., Essaouini, K., Gibelin, A.-L., Giordani, H., Habets, F., Jidane, M., Kerdraon, G., Kourzeneva, E., Lafaysse, M., Lafont, S., Lebeaupin Brossier, C., Lemonsu, A., Mahfouf, J.-F., Marguinaud, P., Mokhtari, M., Morin, S., Pigeon, G., Salgado, R., Seity, Y., Taillefer, F., Tanguy, G., Tulet, P., Vincendon, B., Vionnet, V., and Voldoire, A.: The

SURFEXv7.2 land and ocean surface platform for coupled or offline simulation of earth surface variables and fluxes, Geoscientific Model Development, 6, 929–960, https://doi.org/10.5194/gmd-6-929-2013, 2013.

McKinney, W.: Data Structures for Statistical Computing in Python, in: Proceedings of the 9th Python in Science Conference, edited by van der Walt, S. and Millman, J., https://conference.scipy.org/proceedings/scipy2010/pdfs/mckinney.pdf, 2010.

Met Office: Cartopy: a cartographic python library with a matplotlib interface, http://scitools.org.uk/cartopy, 2015.

Nakanishi, M. and Niino, H.: Development of an Improved Turbulence Closure Model for the Atmospheric Boundary Layer, Journal of the Meteorological Society of Japan. Ser. II, 87, 895–912, https://doi.org/10.2151/jmsj.87.895, 2009.

Neggers, R., Köhler, M., and Beljaars, A.: A dual mass flux framework for boundary layer convection. Part I: Transport, 2007.

Pinty, J.-P. and Jabouille, P.: A mixed-phased cloud parameterization for use in a mesoscale non-hydrostatic model: simulations of a squall line and of orographic precipitation, in: Preprints of Conf. On Cloud Physics, pp. 217–220, Amer. Meteor. Soc, Everett, WA, 1998.

Platis, A., Siedersleben, S. K., Bange, J., Lampert, A., Bärfuss, K., Hankers, R., Cañadillas, B., Foreman, R., Schulz-Stellenfleth, J., Djath, B., Neumann, T., and Emeis, S.: First in situ evidence of wakes in the far field behind offshore wind farms, Scientific Reports, 8, 2163, https://doi.org/10.1038/s41598-018-20389-y, 2018.

Platis, A., Bange, J., Bärfuss, K., Cañadillas, B., Hundhausen, M., Djath, B., Lampert, A., Schulz-Stellenfleth, J., Siedersleben, S., Neumann, T., and Emeis, S.: Long-range modifications of the wind field by offshore wind parks – results of the project WIPAFF, Meteorol Z, https://doi.org/10.1127/metz/2020/1023, 2020.

Pryor, S. C., Shepherd, T. J., Volker, P. J. H., Hahmann, A. N., and Barthelmie, R. J.: "Wind Theft" from Onshore Wind Turbine Arrays: Sensitivity to Wind Farm Parameterization and Resolution, J Appl Meteorol Clim, 59, 153–174, https://doi.org/10.1175/jamc-d-19-0235.1, 2020.

Schlünzen, K. H. and Sokhi, R. S., eds.: Overview of Tools and Methods for meteorological and air pollution mesoscale model evaluation and user training, GAW Report No. 181, World Meteorological Organization, https://library.wmo.int/index.php?lvl=notice_display&id=12628#.YfO4S_sxlhE, 2008.

Shepherd, T. J., Barthelmie, R. J., and Pryor, S. C.: Sensitivity of Wind Turbine Array Downstream Effects to the Parameterization Used in WRF, Journal of Applied Meteorology and Climatology, 59, 333–361, https://doi.org/10.1175/JAMC-D-19-0135.1, 2020.

Siebesma, A. P., Soares, P. M. M., and Teixeira, J.: A Combined Eddy-Diffusivity Mass-Flux Approach for the Convective Boundary Layer, Journal of the Atmospheric Sciences, 64, 1230–1248, https://doi.org/10.1175/JAS3888.1, 2007.

Siedersleben, S. K., Lundquist, J. K., Platis, A., Bange, J., Bärfuss, K., Lampert, A., Cañadillas, B., Neumann, T., and Emeis, S.: Micrometeorological impacts of offshore wind farms as seen in observations and simulations, Environmental Research Letters, 13, 124 012, https://doi.org/10.1088/1748-9326/aaea0b, 2018.

Siedersleben, S. K., Platis, A., Lundquist, J. K., Djath, B., Lampert, A., Bärfuss, K., Cañadillas, B., Schulz-Stellenfleth, J., Bange, J., Neumann, T., and Emeis, S.: Turbulent kinetic energy over large offshore wind farms observed and simulated by the mesoscale model WRF (3.8.1), Geoscientific Model Development, 13, 249–268, https://doi.org/10.5194/gmd-13-249-2020, 2020.

Simmons, A. J. and Burridge, D. M.: An energy and angular-momentum conserving vertical finite- difference scheme and hybrid vertical coordinates., Monthly Weather Review, 109, 758–766, https://doi.org/10.1175/1520-0493(1981)109<0758:AEAAMC>2.0.CO;2, 1981.

Skamarock, W. C., Klemp, J. B., Dudhia, J., Gill, D. O., Liu, Z., Berner, J., Wang, W., Powers, J. G., Duda, M. G., Barker, D., and Huang, X.-y.: A Description of the Advanced Research WRF Model Version 4.1, Tech. rep., https://doi.org/10.5065/1dfh-6p97, 2019.

Tewari, M., Chen, F., Wang, W., Dudhia, J., LeMone, M. A., Mitchell, K., Ek, M., Gayno, G., Wegiel, J., and Cuenca, R. H.: Implementation and verification of the unified NOAH land surface model in the WRF model, 20th conference on weather analysis and forecasting/16th conference on numerical weather prediction, https://www2.mmm.ucar.edu/wrf/users/physics/phys_refs/LAND_SURFACE/noah.pdf, 2004.

Thompson, G., Field, P. R., Rasmussen, R. M., and Hall, W. D.: Explicit Forecasts of Winter Precipitation Using an Improved Bulk Microphysics Scheme. Part II: Implementation of a New Snow Parameterization, Monthly Weather Review, 136, 5095–5115, https://doi.org/10.1175/2008MWR2387.1, 2008.

van der Walt, S., Colbert, S. C., and Varoquaux, G.: The NumPy Array: A Structure for Efficient Numerical Computation, Computing in Science & Engineering, 13, 22–30, https://doi.org/10.1109/MCSE.2011.37, 2011.

van Stratum, B., Theeuwes, N., Barkmeijer, J., van Ulft, B., and Wijnant, I.: A One-Year-Long Evaluation of a Wind-Farm Parameterization in HARMONIE-AROME, Journal of Advances in Modeling Earth Systems, 14, https://doi.org/10.1029/2021MS002947, 2022.

Volker, P. J., Badger, J., Hahmann, A. N., and Ott, S.: The explicit wake parametrisation V1.0: A wind farm parametrisation in the mesoscale model WRF, Geoscientific Model Development, 8, 3715–3731, https://doi.org/10.5194/gmd-8-3715-2015, 2015.

Volker, P. J. H., Hahmann, A. N., Badger, J., and Jørgensen, H. E.: Prospects for generating electricity by large onshore and offshore wind farms, Environmental Research Letters, 12, 034 022, https://doi.org/10.1088/1748-9326/aa5d86, 2017.

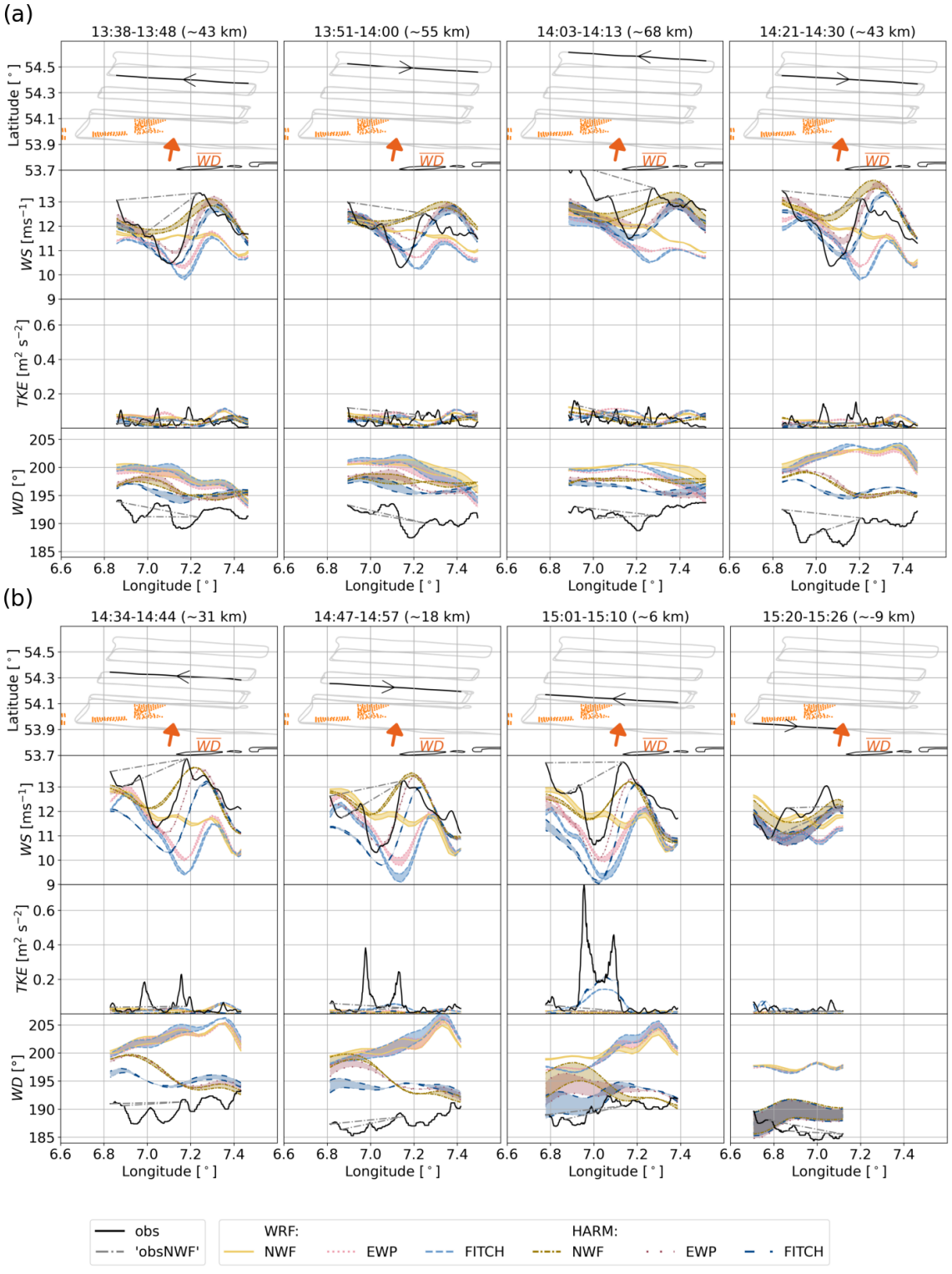

Figure A1. As Fig. 8, but for 15 October 2017 and for around 120 m height for later flight transects as those shown in Fig. 11.

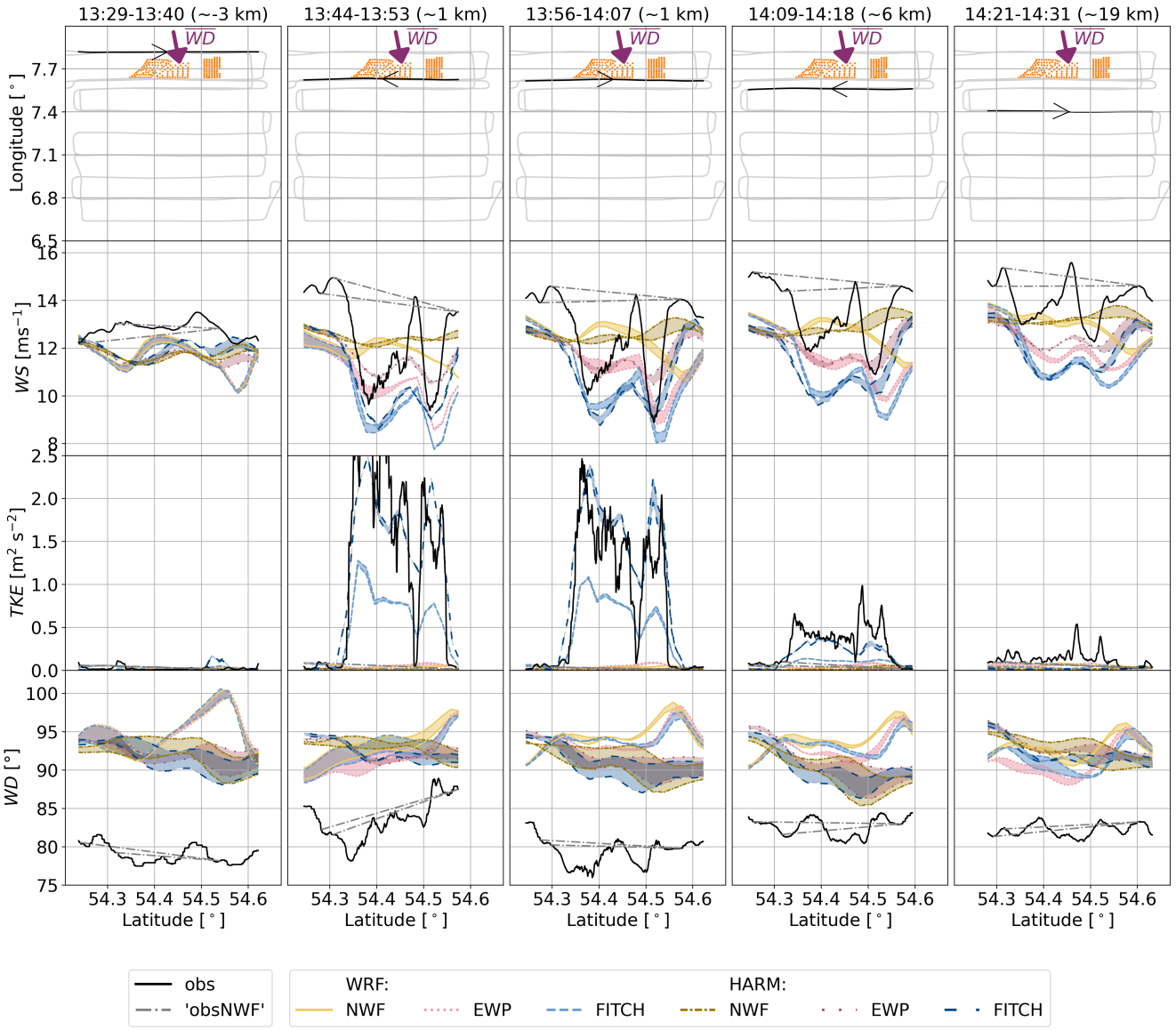

Figure A2. As Fig. 8, but for 08 August 2017 and for around 90 m height.